MENTATION PAGE

Form Approved
OMB No 0704-0188

1. AGENCY USE ONLY (Leave blank)	2. REPORT DATE	3. REPORT TYPE AND DATES COVERED
	4/27/92	Final, 7Feb89 - 28Feb92

4. TITLE AND SUBTITLE

Micromechanisms of Deformation and Fracture in Aluminum Based MMCs - Interface Effects

5. FUNDING NUMBERS

DAAL03-89-K-0068

6. AUTHOR(S)

Professor John J. Lewandowski

7. PERFORMING ORGANIZATION NAME(S) AND ADDRESS(ES)

John J. Lewandowski
Department of Materials Science and Engineering
Case Western Reserve University
Cleveland, Ohio 44106

8. PERFORMING ORGANIZATION REPORT NUMBER

9. SPONSORING/MONITORING AGENCY NAME(S) AND ADDRESS(ES)

U. S. Army Research Office
P. O. Box 12211
Research Triangle Park, NC 27709-2211

10. SPONSORING/MONITORING AGENCY REPORT NUMBER

ARO 25390.9-MS

11. SUPPLEMENTARY NOTES

The view, opinions and/or findings contained in this report are those of the author(s) and should not be construed as an official Department of the Army position, policy, or decision, unless so designated by other documentation.

12a. DISTRIBUTION/AVAILABILITY STATEMENT

Approved for public release; distribution unlimited.

12b. DISTRIBUTION CODE

13. ABSTRACT *(Maximum 200 words)*

Microstructural effects on the deformation and fracture of Aluminum-based metal matrix composites have been determined. Microstructural variables investigated included the reinforcement size, volume fraction, and matrix microstructure. Reinforcement sizes studied included 5 um and 13 um SiC particulates at both the 15 and 20 volume percent levels. Matrix microstructures were systematically varied via heat treatment and were quantified using transmission electron microscopy. Fracture toughness was evaluated using J-integral test techniques and utilized in-situ monitoring of fracture inside a Scanning Electron Microscope. Mixed mode fracture toughness tests were also conducted. In addition to the fracture toughness tests, additional tests were conducted on specimens deformed under high pressure. The composites exhibited high ductilty under pressure (e.g. e_f = 80%). Laminated composites were additionally processed and exhibited significant improvements in both bend ductility and fracture toughness.

14. SUBJECT TERMS	15. NUMBER OF PAGES
Metal Matrix Composites, Toughness, Laminates, Microstructure Effects, Ductility	35
	16. PRICE CODE

17. SECURITY CLASSIFICATION OF REPORT	18. SECURITY CLASSIFICATION OF THIS PAGE	19. SECURITY CLASSIFICATION OF ABSTRACT	20. LIMITATION OF ABSTRACT
UNCLASSIFIED	UNCLASSIFIED	UNCLASSIFIED	UL

MICROMECHANISMS OF DEFORMATION AND FRACTURE IN ALUMINUM BASED MMCs - INTERFACE EFFECTS

FINAL REPORT

PROF. JOHN J. LEWANDOWSKI

APRIL 27, 1992

U.S. ARMY RESEARCH OFFICE

ARO-DAAL03-89-K0068

CASE WESTERN RESERVE UNIVERSITY
DEPT. MATERIALS SCIENCE AND ENGINEERING
CLEVELAND, OHIO 44106

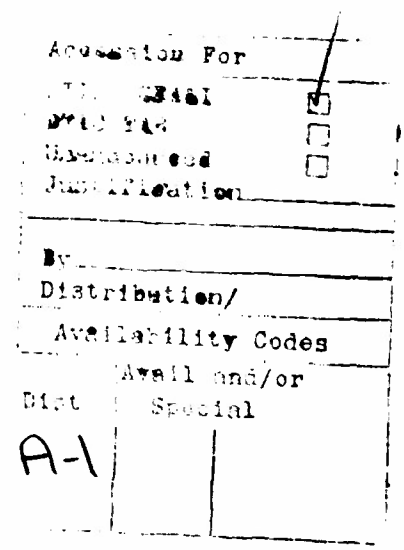

APPROVED FOR PUBLIC RELEASE;

DISTRIBUTION UNLIMITED.

A. STATEMENT OF THE PROBLEMS STUDIED

1. Optimize the Properties of Aluminum Metal Matrix Composites (MMCs) through changes in reinforcement size, volume fraction, and changes in heat treatment.

2. Determine the effects of changes in reinforcement particulate size and volume fraction on the tensile properties and fracture toughness. Reinforcement volume fractions of 15% and 20% were studied, while SiC particle sizes of 5 um and 13 um were studied.

3. Determine the effects of heat treatment on the tensile properties and fracture toughness of particulate reinforced MMCs.

4. Investigate the effects of high pressure deformation on the subsequent ductility and fracture behavior.

5. Explore the possibility of producing low cost laminated MMCs which possess a combination of high ductility, high strength and modulus, and high toughness.

B. SUMMARY OF THE MOST IMPORTANT RESULTS

1. The properties of the MMCs investigated included Aluminum Alloy MMCs consisting of either an Al-Zn-Mg-Cu matrix or an Al-Mg-Cu matrix. The properties of the monolithic materials were studied in addition to the composites. It was shown that an underaged heat treatment with a 13 um average SiC particle size produced the best combination of mechanical properties in the composite. Significant effects of heat treatment on the fracture mechanisms and resulting properties were documented and related to the details of the matrix/reinforcement interface.

2. It is shown that the 13 um SiC particulate composites exhibited better properties than the composites containing the 5 um SiC particles. The composites containing 15 volume percent SiC exhibited better fracture properties but lower elastic modulus than the composites containing 20 volume percent SiC particulates.

3. Heat treatment was shown to have a dramatic effect on the tensile and fracture toughness of the composites. Microstructures were characterized with Transmission Electron Microscopy and the sources of the large effects of heat treatment on properties were identified. Significant changes in the SiC/matrix interface were observed with heat treatment. The nature of the segregation at the interface was quantified.

4. Deformation conducted with high pressure was shown to dramatically increase the ductility and fracture properties of the composites. It was shown that the matrix microstructure and matrix alloy exert a major effect on the behavior under high pressure conditions.

5. Preliminary studies were conducted to produce low cost laminated composites with improved strength and toughness. Laminates were processed to contain alternating layers of composite and monolithic aluminum alloy, followed by a determination of fracture toughness and bend toughness. Dramatic increases in the fracture related properties were obtained, with increases in toughness in excess of 200% depending on the orientation of the laminates.

C. LIST OF ALL PUBLICATIONS AND TECHNICAL REPORTS

1. M. Manoharan and J.J. Lewandowski, "In-situ Deformation Studies of an Aluminum Metal Matrix Composite in a Scanning Electron Microscope", Scripta Metallurgica, 23, pp. 1801-1804, 1989.

2. D.S. Liu, M. Manoharan, and J.J. Lewandowski, "Matrix Effects on the Ductility of Aluminum Matrix Composites Tested Under Hydrostatic Pressure", Jnl. of Materials Science Letters, 8, pp. 1447-1449, 1989.

3. M. Manoharan and J.J. Lewandowski, "Crack Initiation and Growth Toughness in an Aluminum Metal Matrix Composite", Acta Metallurgica, 38, pp. 489-96, 1990.

4. M. Manoharan and J.J. Lewandowski, "Microstructural Effects on the Toughness of Aluminum Alloy Based Metal Matrix Composites", in Fundamental Relationships Between Microstructures and Mechanical Properties of Metal Matrix Composites, (M.N. Gungor and P.K. Liaw, eds.) TMS-AIME, Warrendale, PA, pp. 471-479, 1990.

5. L. Ellis and J.J. Lewandowski, "Laminated Composites with Improved Bend Ductility and Toughness", Journal of Materials Science Letters, 10, pp. 461-463, 1990.

6. M. Manoharan, L. Ellis, and J.J. Lewandowski, "Laminated Composites with Improved Toughness", Scripta Metallurgica, 24, pp. 1515-1519, 1990.

7. M. Manoharan and J.J. Lewandowski, "Combined Mode I-Mode III Fracture Toughness of a Particulate Reinforced Metal Matrix Composite, Journal of Composite Materials, 25, pp. 831-842, 1991.

8. M. Manoharan and J.J. Lewandowski, "Effects of Reinforcement Size and Matrix Microstructure on the Fracture Properties of an Aluminum Metal Matrix Composite", Materials Science and Engineering, A150, pp. 179-186, 1992.

9. T. Osman and J.J. Lewandowski, "Impact Performance of Laminated Composites", in preparation.

10. L. Ellis, "Effects of Lamination on the Fracture Properties of Metal Matrix Composites", M.S. Thesis, Case Western Reserve University, in press, 1992.

11. T. Osman, "Effects of Interface Strength and Processing Conditions on the Fracture Properties of Laminated MMCs", M.S. Thesis, Case Western Reserve University, in press, 1992.

D. PARTICIPATING SCIENTIFIC PERSONNEL

1. Dr. M. Manoharan - Post Doctoral Researcher

2. Ms. Lisa Yost Ellis - M.S. Candidate, Expected Completion 8/92.

3. Mr. Todd Osman - M.S. Candidate, Expected Completion, 8/92.

APPENDIXES

Papers published under the supported period are included in this report..

Scripta METALLURGICA Vol. 23, pp. 1801-1804, 1989
Printed in the U.S.A.

IN-SITU DEFORMATION STUDIES OF AN ALUMINUM METAL-MATRIX COMPOSITE IN A SCANNING ELECTRON MICROSCOPE

M. Manoharan and J.J. Lewandowski
Department of Materials Science and Engineering
Case Western Reserve University
Cleveland, Ohio - 44106

(Received July 10, 1989)
(Revised August 15, 1989)

Introduction

Metal-matrix composites have been developed in recent years to fulfill the need for materials with high specific strength and stiffness. Fiber reinforced composites provide the highest improvements in strength and stiffness in the reinforcement direction. Particulate reinforced metal-matrix composites, on the other hand, provide more isotropic properties and can be formed using conventional metal deformation processes.

The use of metal-matrix composites as structural materials depends to some extent on their degree of damage tolerance. The initiation fracture toughness of these composites have generally been evaluated using linear elastic (K_{Ic}) fracture parameters (1,2). However, recent studies (3) have shown that aluminum based metal matrix composites fracture by stable crack growth and the energy absorbed during crack propagation is a significant fraction of the total energy of fracture. In a 7091 aluminum composite crack initiation has been characterized by J_{Ic} and crack propagation by the tearing modulus (3).

In the fracture toughness tests reported elsewhere (3), crack propagation was monitored optically using a travelling microscope fitted to a stage equipped with a LVDT. For this purpose, the external surfaces of the specimens were polished metallographically, and the details of crack propagation were studied in-situ with the use of a high power optical microscope (magnification 500 X) connected to a video recording system. In-situ measurements were similarly made on specimens designed to permit controlled propagation of a crack, as reported elsewhere (4). These observations (3,4) suggested that microcracking occurred ahead of the crack-tip, which could also contribute to energy absorption during fracture. Tensile specimens were tested in-situ in a scanning electron microscope equipped with a deformation stage to directly observe these phenomena.

Experimental Procedures

The material studied was a cast and extruded aluminum alloy based, particulate reinforced metal matrix composite. The matrix was a 6061 aluminum alloy and the reinforcement consisted of 15 % by volume of Al_2O_3 particulate of average size 15 μm. The composite was solution treated at 520^{0}C for 4 hours and then artificially aged at 175^{0}C for 100 hours to produce an overaged (OA) microstructure.

Fracture toughness tests were conducted on fatigue precracked three point bend specimens in general accordance with the applicable ASTM standard E-399 for evaluation of K_{Ic}. A schematic of the three point bend specimen is shown in Fig. 1. In-situ deformation studies were conducted on tensile samples of type shown in Fig. 2. This was accomplished using a JEOL 840 A Scanning Electron Microscope equipped with a deformation stage. This deformation stage is capable of applying tensile or compressive loads to a maximum of 80 kgf on suitably designed specimens. The unit allows in-situ SEM observation of a metallographically polished surface of a specimen at various points in the load-displacement curve. Increasing tensile loads were applied to the specimen under displacement control until a crack was initiated in the gage section. Once the crack was initiated, the crack tip region was continuously monitored and the crack path studied.

0036-9748/89 $3.00 + .00

Results and Discussion

From the uniaxial tensile tests the following tensile properties were determined for the composite : yield strength - 285 MPa, ultimate tensile strength - 325 MPa and reduction in area - 16 %. A typical plot of the load-crack opening displacement curve during a fracture toughness test is shown in Fig. 3. It can be seen that the load increases continuously until a maximum is reached. The load for calculating K_{Ic} was arrived at using the procedure outlined in ASTM E-399. It can be seen that once the crack initiated at this load, stable crack growth ensued with a smooth drop in the load as displacement increased. Since the area under the load-discplacement curve is a measure of the energy of fracture, it is obvious that a significant amount of energy is absorbed during crack propagation. Research is currently underway to characterize the crack growth toughness using tearing modulus (5). It was observed in these tests and in other tests on similar composites (4) that microcracking occurred ahead of the crack tip as the crack progressed . In the present case these microcracks were primarily associated with cracks in the alumina particles.

The in-situ SEM deformation studies also revealed the presence of microcracks both ahead of and near the crack tip region. Fig. 4 shows a low magnification view of the crack in the tensile specimen. Figs. 5-7 illustrate three steps in the deformation process once the macroscopic crack has initiated. It can be seen in Fig. 5 that there are a number of microcracks (e.g. 'b', 'c') ahead of and near the crack tip (denoted 'a'). In Fig. 6 the crack propagation is shown to occur by a process whereby some of these microcracks ('b') join via matrix failure ahead of the original crack tip, concurrent with the initiation of additional microcracks ahead of the crack. Fig. 7 illustrates further crack growth by similar phenomena. These figures would suggest that a region of intense deformation exists ahead of the crack and in these composites corresponds to the region of microcracking. As the crack progresses, it is apparent that a region of plastically deformed material and associated microcracks remain in the wake of the crack as illustrated by Fig. 8 which shows a region near the fracture surface after the crack has passed through.

The extent of the region of intense plastic flow and associated microcracing is consistent with earlier work on similar composites (4). Using a model developed originally by Rice and Johnson (6), Kamat et. al. (2) estimated the extent of the region of intense straining ahead of a crack tip from a knowledge of K_{Ic} and yield stress of a aluminum based particulate metal-matrix composite. They concluded that the extent of this region is comparable to the spacing between the reinforcements in their composites which exhibited stable crack propagation. The in-situ observations reported in this study shed additional light on the micromechanical events involved in the fracture process of the composites tested presently. In the present case, it is apparent that microcracking ahead of the crack tip occurs in a region considerably larger than the inter-particle spacing. However, the macrocrack seems to link up with the microcracks ahead of it when the distance between them is comparable to interparticle spacing, as illustrated in Fig. 6, compatible with the model.

Acknowledgements

This work was partially supported by the U.S. Army Research Office (JJL) and by NASA NAGW 1193 (MM, JJL).

References

1. M. Manoharan and J.J. Lewandowski, Scripta Metall., **23** , (1989), p.301.
2. S.V. Kamat, J.P. Hirth and R. Mehrabian, Acta Metall., (1989) in press.
3. M. Manoharan and J.J. Lewandowski, Acta Metall., Submitted.
4. J.J. Lewandowski, C. Liu and W.H. Hunt Jr., Mat. Sci. Engr., **A107** , (1989), p. 241.
5. M. Manoharan and J.J. Lewandowski, Unpublised research.
6. J.R. Rice and M.A. Johnson, 'Inelastic Behavior of Solids', M.F. Kanninen et. al. eds., McGraw-Hill, New York, (1969), p. 641.

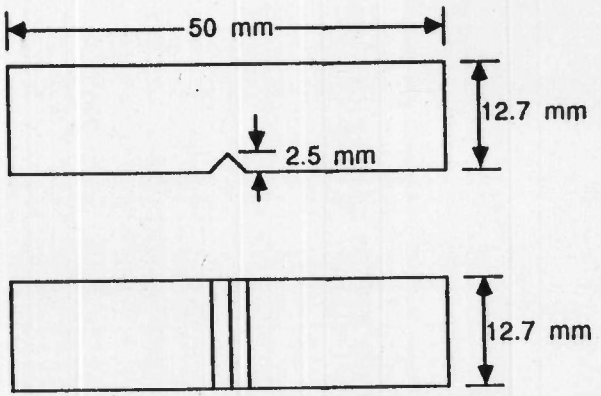

Fig. 1 : Three Point Bend Specimen Used in Fracture Toughness Tests.

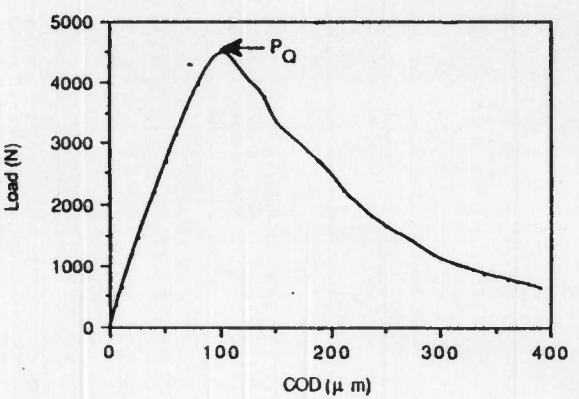

Fig. 3 : Load-COD Curve in Fracture Toughness Tests.

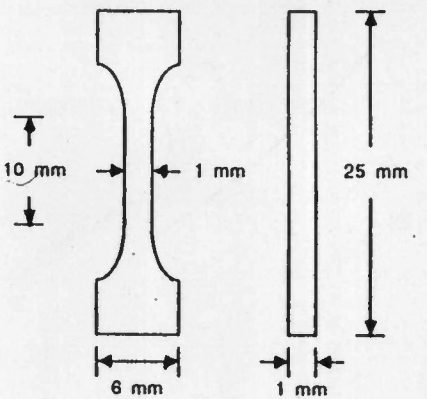

Fig. 2 : Tensile Specimen Used in In-situ Deformation studies.

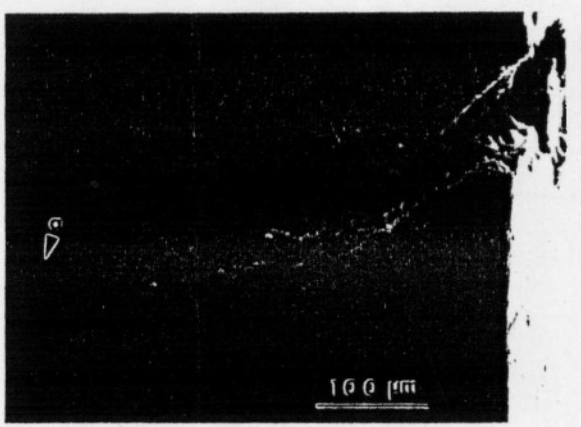

Fig. 4 : Low Magnification View of Crack in Tensile Specimen.

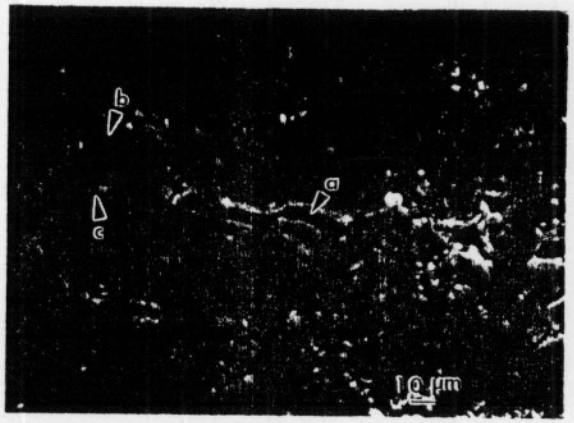

Fig. 5 : Microcracks Near and Ahead of Crack Tip.

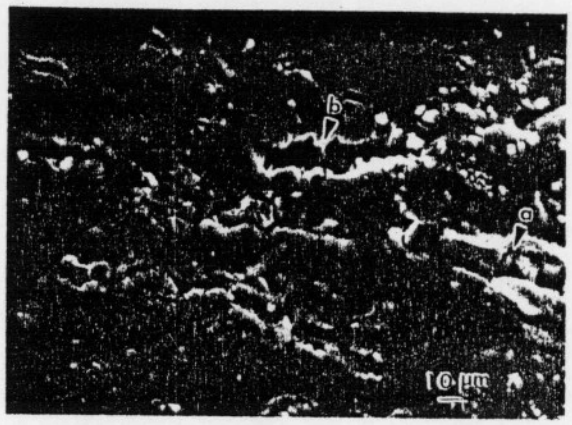

Fig. 6 : Link-up of Microcracks with Macrocrack.

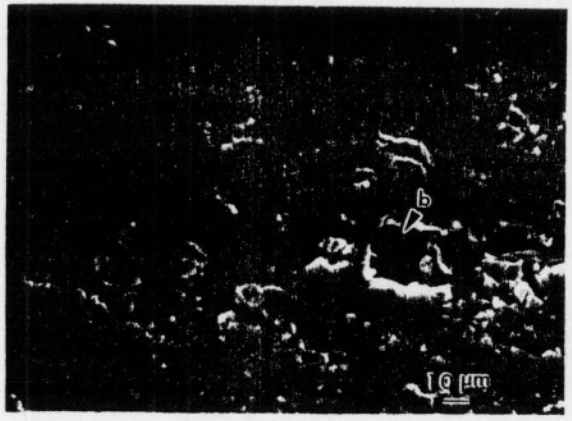

Fig. 7 : A Further Step in the Crack Growth Process.

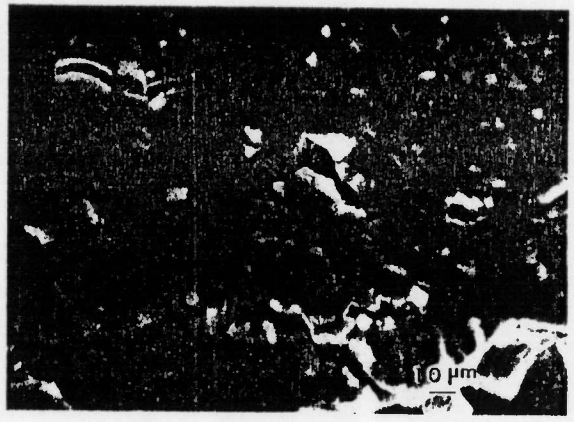

Fig. 8 : Microcracks Near Fracture Surface.

JOURNAL OF MATERIALS SCIENCE LETTERS 8 (1989) 1447–1448

Matrix effects on the ductility of aluminium-based composites deformed under hydrostatic pressure

D. S. LIU, M. MANOHARAN, J. J. LEWANDOWSKI
Department of Materials Science and Engineering, Case Western Reserve University, Cleveland, Ohio 44106, USA

Metal matrix composites have received increased attention in recent years due to the need for high-strength materials in various structural applications. The addition of a fairly strong and brittle reinforcement to a metal serves to improve the strength and stiffness, but the ductility of the composite is typically lower than that of the unreinforced matrix [1, 2]. This is consistent with observations of reduced ductility accompanying increased volume fractions of reinforcements or inclusions in ductile matrices [3].

The superimposition of compressive hydrostatic stresses provides increased ductility in these materials [4, 5], and approximates the stress state obtained in various material-forming applications. Furthermore, the relatively low ductiles of these composites complicates the detailed study of the damage events leading to catastrophic fracture. The enhancement of ductility provided by superimposing hydrostatic pressure during deformation provides an improved means of studying the fracture micromechanisms in these materials.

There has been relatively little work on the effects of superimposed hydrostatic pressure on the deformation behaviour of composites. Recent work on aluminium alloy composites [4–6] and on Al–Ni composites [6] has revealed a significant effect of superimposed hydrostatic pressure on the ductility of these materials. Previous studies have not, however, focused on the effects of the matrix alloy composition and ageing condition on the pressure-induced ductility response of these materials.

Composites based on three different matrix compositions were studied in this investigation. The first composite material studied was a powder metallurgy 2XXX series aluminium alloy, designated MB-85, containing (in wt %) 3.5 copper, 1.5 magnesium, 0.4 zirconium, 0.21 manganese, balance aluminium, reinforced with 15 vol % SiC particulate (average size 13 μm). Processing details are summarized elsewhere [1, 2]. The second composite was a 6061 aluminium alloy containing 15 vol % Al_2O_3 particulate (average size 13 μm), and the third was a 7XXX series aluminium alloy designated MB-78, containing (in wt %) 7 zinc, 2 magnesium, 2 copper, 0.14 zirconium, balance aluminium, reinforced with 15 vol % SiC particulate (average size 13 μm).

Heat treatments were designed to produce underaged (UA) and overaged (OA) microstructures possessing equivalent values of yield strength and matrix microhardness for both the composite materials. Heat treatments for the 7XXX and 2XXX series composites

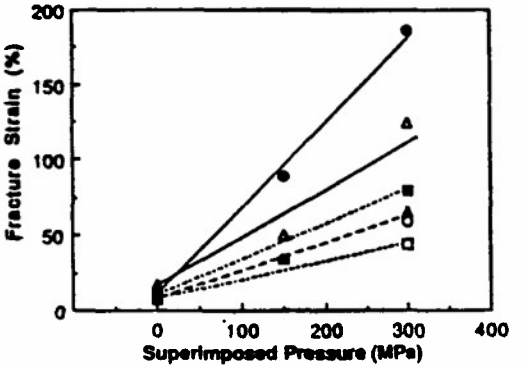

Figure 1 Fracture strain plotted against superimposed hydrostatic pressure. (○, ●) 2XXX UA and OA, (△, ▲) 6XXX UA and OA, and (□, ■) 7XXX UA and OA, respectively.

are summarized in [1, 2, 4, 5], and for the 6061 composite the heat treatment was as follows. Solution treatment was conducted at 510° C for 4 h, followed by artificial ageing at 175° C for 2 h for the UA condition, and at 175° C for 100 h for the OA condition.

Tensile testing was conducted to failure at a constant displacement rate of 0.2 mm min^{-1} on smooth cylindrical tensile specimens of gauge length 15.2 mm and diameter 3.8 mm at atmospheric pressure and under superimposed hydrostatic confining pressures of either 150 or 300 MPa. The pressures chosen for this study were selected to be less than or comparable with the flow stress of the monolithic matrix materials. Tensile testing at atmospheric pressure was conducted on an Instron Model 1125 universal testing machine, and those performed under superimposed hydrostatic compression were conducted in our high-pressure laboratory, as described in [4, 5].

Fracture surfaces, the polished external specimen

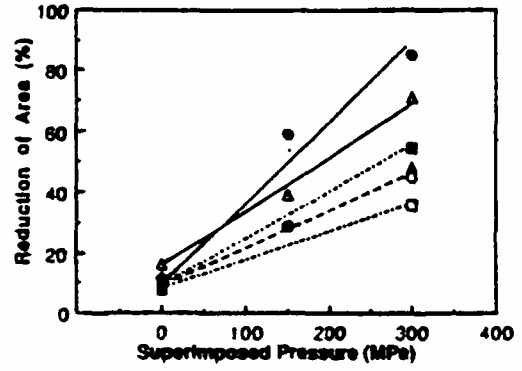

Figure 2 Reduction in area plotted against superimposed hydrostatic pressure. (○, ●) 2XXX UA and OA, (△, ▲) 6XXX UA and OA, and (□, ■) 7XXX UA and OA, respectively.

0261–8028/89 $03.00 + .12

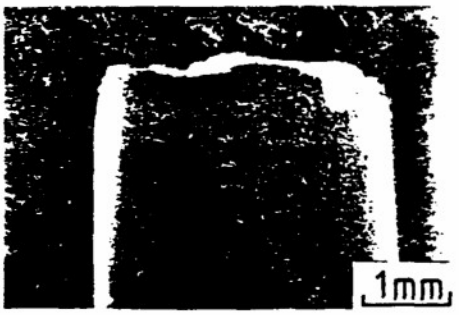

Figure 3 Atmospheric pressure test revealing low-ductility fracture.

Figure 4 Test conducted at 300 MPa superimposed hydrostatic pressure exhibiting significant reduction in area.

surfaces and polished longitudinal sections were examined on a Jeol 35CF scanning electron microscope (SEM) operated at 25 kV. After SEM examination of the failed specimens, the fracture strains and reduction in areas were measured using an optical comparator, where the broken halves of the specimens were fitted together to enable measurement of specimen dimensions. A number of readings were taken along the circumference of the neck, and these were then averaged.

The effects of superimposed hydrostatic pressure on the ductility as measured by fracture strain and reduction in area are summarized in Figs 1 and 2. Fig. 1 illustrates the change in ductility as a function of the superimposed hydrostatic pressure for the three composites with different matrix alloy compositions. Although the ductilities at atmospheric pressure are nearly equivalent for the cases tested, the ductility response to pressure in the 2XXX and 7XXX series composites is lower than that in the 6061 composite for both of the ageing conditions studied. Furthermore, although the response of the 2XXX composite is nearly identical for both of the ageing conditions, the OA material was observed to be more sensitive to superimposed hydrostatic pressure in the 6061 and 7XXX composites. The reduction in area shows a dependence on pressure similar to that obtained in the measurements of the fracture strains for the composites tested.

Representative macroscopic views showing specimens fractured both at atmospheric pressure and at 300 MPa superimposed hydrostatic pressure are shown in Figs 3 and 4. This illustrates the significant effect of pressure on ductility in these composites.

The magnitude of ductility increase in response to superimposed hydrostatic pressure seems to be significantly affected by the ratio of the superimposed pressure to the flow stress of the matrix, as well as by the details of the matrix microstructure. To the authors' knowledge these effects have not previously been reported. Work is continuing to investigate the mechanism controlling the accumulation of damage in these materials [7].

Acknowledgements

The authors appreciate the assistance of those involved with the high-pressure laboratory at Case Western Reserve University. Support for this work was provided by CSIST (DSL), the US Army Research Office (JJL), with partial experimental support from DARPA-ONR-N00013-86-K-0773.

References

1. J. J. LEWANDOWSKI, C. LIU and W. H. HUNT, JR. in "Powder Metallurgy Composites", edited by M. Kumar, K. Vedula and A. M. Ritter (TMS-AIME, Warrendale, Pennsylvania, 1987) p. 117.
2. *Idem, Mater. Sci. Engng.* **A107** (1989) 241.
3. B. EDELSON and W. BALDWIN, *Trans. Amer. Soc. Metals* **55** (1962) 230.
4. D. S. LIU, M. MANOHARAN and J. J. LEWANDOWSKI, *Scripta Metall.* **23** (1989) 253.
5. *Idem, Metall. Trans. A* (1988) submitted.
6. F. ZOK, J. D. EMBURY, M. F. ASHBY and O. RICHMOND, in Ninth Risø International Symposium on Metallurgy and Materials Science, edited by S. I. Anderson, H. Lilholt and O. B. Pederson (Risø National Laboratory, 1989) in press.
7. D. S. LIU, M. MANOHARAN and J. J. LEWANDOWSKI, unpublished research.

Received 4 April
and accepted 17 May 1989

Acta metall. mater. Vol. 38, No. 3, pp. 489–496, 1990
Printed in Great Britain.

0956-7151/90 $3.00 + 0.00

CRACK INITIATION AND GROWTH TOUGHNESS OF AN ALUMINUM METAL–MATRIX COMPOSITE

M. MANOHARAN and J. J. LEWANDOWSKI

Department of Materials Science and Engineering, Case Western Reserve University, Cleveland, OH 44106, U.S.A.

(*Received* 22 *May* 1989)

Abstract—The effects of systematic changes in matrix microstructure on crack initiation and growth toughnesses were determined on an Al–Zn–Mg–Cu alloy containing 0, 15, 20% by volume of SiC particulates. Materials were heat treated to underaged (UA) and overaged (OA) conditions of equivalent matrix microhardness and flow stress. Although both the fracture initiation and growth toughnesses, as measured by J_{Ic} and tearing modulus, were similar for the unreinforced materials in the UA and OA conditions, significant effects of microstructure on both J_{Ic} and tearing modulus were observed in the composites. SEM and TEM observations of fracture paths in the two conditions are utilized to rationalize these observations in light of existing theories of ductile fracture propagation.

Résumé—L'effet de variations systématiques de la microstructure de la matrice sur la résistance à l'initiation et à la croissance des fissures a été déterminé dans un alliage Al–Zn–Mg–Cu contenant 0, 15 ou 20% en volume de particules de SiC. Les matériaux ont subi des traitement thermiques pur atteindre des conditions de sous-vieillisement ou de survieillissement donnant des microduretés et des contraintes d'écoulement équivalentes de la matrica. Bien que les résistances à l'initiation comme à la croissance des fissures, telles qu'elles sont mesurées par J_{Ia} et par le module de déchirement, soient semblables pour les matériaux non renforcès dans les conditions de sur- et de sous-vieillissement, on observe, dans les composites, un effet marquè de la microstruture à la fois sur J_{Ic} et sur le module de déchirement. Les observations, en microscopie électronique à balayage ou en transmission, des chemins de rupture dans les deux cas permettent de rationliser ces observations à la lumière des théories actuelles de la propagation de la rupture ductile.

Zusammenfassung—Die Einfluß systematischer Veränderungen in der Mikrostruktur der Matrix auf Rißeginn und Wachstumszähigkeit wurde en einer Al–Zn–Mg–Cu-Legierung mit 0, 15 und 20 vol.-% SiC-Teilchen untersucht. Die Proben wurden wärmebehandelt, um unter- und überalterte Bedingungen bei sonst gleichwertigen Werten der Mikrohärte und der Fließspannung der Matrix zu erhalten. Bei den nicht verstärkten Proben waren Bruchbeginn und Wachstumszähigkeit, gemessen mit J_{Ic} und Zerreißmodul, für den unter- und überalteren Zustand ähnlich. In den anderen Proben wurde ein beträchtlicher Einfluß der Mikrostruktur auf J_{Ic} und Zerreißmodul beobachtet. Beobachtungen im Raster- und im Durchstrahlungselektronenmikroskop zu den Bruchwegen in beiden Zuständen werden benutzt, um diese Befunde anhand bestehender Theorien der duktilen Rißausbreitung zu beschreiben.

1. INTRODUCTION

The development of metal matrix composites has been catalyzed by the necd for structural materials with high specific strength and stiffness. Reinforcements may be continuous in the form of fiber or discontinuous in the form of whiskers or particulates. While fiber reinforced composites offer the highest specific stiffness along the reinforcement direction, particulate reinforced composites are more isotropic in their properties and are also easier to process, via powder metallurgy or casting routes.

The mechanical properties of these composites are of primary importance in design considerations when these composites are used as structural materials. Fracture properties of composites are essential in assessing the flaw tolerance of these structures. While there has been some work in evaluating the effects of reinforcement size and volume fraction on the fracture properties of composites based on aluminum matrices [1–3] and Al–Cu–Mg matrices in the annealed condition [2], relatively few studies have focussed on the effects of matrix microstructure. Recent studies [3, 4] have, however, indicated significant effects of matrix microstructure on the fracture micro-mechanisms in composites based on Al–Zn–Mg–Cu matrices.

The principal objectives of the current investigation were to evaluate the effects of systematic changes in microstructure and reinforcement volume fraction on the fracture initiation and growth toughness of a SiC particulate reinforced aluminum alloy based metal matrix composite. The age hardenable matrix permitted the evaluation of underaged and overaged matrix microstructures of equivalent tensile properties for both the unreinforced alloy and the composite. It will be shown that while the fracture initiation and growth toughnesses of the monolithic material were only slightly affected by changes in matrix microstructure, dramatically different fracture initiation and growth toughnesses were obtained for the two microstructures in the composite material.

These results are discussed in light of the effects of the local fracture micromechanisms on the macroscopic fracture toughness of these materials.

2. EXPERIMENTAL

The powder metallurgy matrix alloy composition used in this work, contains 7% Zn, 2% Cu, 2% Mg and 0.14% Zr, balance Al. Composites based on this matrix alloy and containing either 15 or 20% by volume of F-600 grade (average size prior to blending = 13 μm) SiC particulate were also obtained. Additional details of the processing of this material via powder metallurgy techniques can be found elsewhere [3, 4]. The as-extruded materials were solution heat treated at 500°C/4 h, cold water quenched, and artificially aged. The aging treatments were selected to provide equivalent matrix microhardnesses ($H_v = 140$ with 30 g load) and 0.2% offset yield strengths in the composite for both the underaged (UA) and overaged (OA) conditions. Aging to the underaged (UA) temper was conducted at 120°C/20 min, while the overaged (OA) temper was produced by a double aging treatment: 120°C/24 h, followed by 170°C/36 h.

The tensile tests were conducted to failure at a constant displacement rate of 0.2 mm/min (i.e. strain rate = 1.3×10^{-4}/s) on smooth cylindrical tensile specimens of gage length 25.4 mm and diameter 6.25 mm using an Instron Model 1125 Universal Testing Machine.

Fracture properties were evaluated in general accordance with the standard procedure for J testing, ASTM E-813-81 [5]. Two types of specimens were used in this study for evaluating the J–R curve. The unreinforced alloy was tested using a three point bend specimen, as shown in Fig. 1. The initial notch was 2.5 mm deep and a fatigue precrack was started from this notch and grown in accordance with ASTM E-813-81. The crack length was continuously monitored using an electrical potential drop system. The calibration curve used to convert potential drop values to equivalent crack length values was based on previous work on similar specimens [6].

The composite was tested using a compact tension specimen geometry, as shown in Fig. 2. A precrack of nominal root radius 30 μm was introduced using a high speed wire saw. Our earlier work [7] had shown

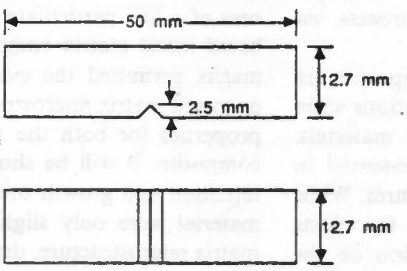

Fig. 1. Schematic of three point bend specimen.

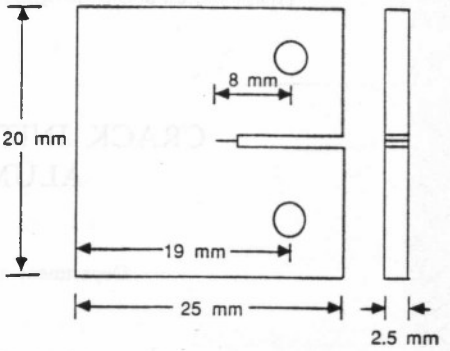

Fig. 2. Schematic of compact tension specimen.

that fracture toughness results obtained using this notch root radius were equivalent to the results using a fatigue precrack. The crack was followed optically using a travelling microscope fitted to a stage equipped with a LVDT. For this purpose, one external surface of each specimen was polished metallographically, and the details of crack propagation were studied *in situ* with the use of a high power optical microscope connected to a video recording system.

The testing for both the bend specimens and the compact tension specimens was carried out on a MTS servo-hydraulic test system operated under stroke control at a crosshead speed of 25 μm/min. In the compact tension specimens, displacement was measured across the crack mouth using a clip-gage mounted between knife edges affixed to the front of the specimen. Load–line displacement for the three point bend specimens was measured taking into account machine compliance in accordance with the ASTM-E-813-81. The load, displacement and crack length data (from LVDT or potential drop) were continuously input and stored in a PDP-11 computer.

J was calculated using the equation

$$J = \frac{A}{Bb} f(a_0/W) \tag{1}$$

where

A = area under the load–displacement record
B = specimen thickness
b = initial uncracked ligament
a_0 = original crack size including fatigue precrack
$f(a_0/W)$ = a geometry dependent constant, from ASTM-E-813-81.

The standard procedure for plane strain J-integral estimation, ASTM E-813-81, was followed for the construction of the J resistance curve. This procedure involves the assumption that the blunting behavior followed the relation, $J = 2\sigma_f \Delta a$, where the flow stress σ_f was set equal to $(\sigma_y + \sigma_u)/2$. The exclusion lines were then drawn at offsets of 0.15 and 1.5 mm, respectively, parallel to the blunting line. The points that lie within these exclusion lines represent valid

data points as they correspond to stable ductile crack extension. A computer program performed a linear regression analysis and fitted a straight line to these data points. The program then determined the exact point of intersection of this straight line with the blunting line and the value of J at the intersection was taken as J_{Qc}.

Once J_{Qc} is determined, it can be verified whether conditions of plane strain are satisfied. ASTME-E-813-81 prescribes that plane strain conditions prevail and the valid J_{Ic} had been obtained if the following conditions are satisfied.

$$B, b > 25J_{Ic}/\sigma_f. \tag{2}$$

where B is the net thickness, b is the uncracked ligament length and σ_f is the effective flow strength. All tests conducted in this study satisfied these criteria for valid J measurement.

The crack initiation behavior of the material under these conditions is thus characterized by the values of J_{Ic}. In addition to determining J_{Ic} it was noted that in all the tests conducted presently, the J–R curve had a non-zero positive slope. The crack propagation behavior was characterized by the tearing modulus concept of Paris *et al.* [8]. The dimensionless value of tearing modulus is given by the expression

$$T = \frac{E}{\sigma_f^2}\frac{dJ}{da} \tag{3}$$

where

dJ/da = slope of the J resistance curve between Δ_c and Δ_{exc}
E = Young's modulus of the material
σ_f = flow stress of the material in tension = $(\sigma_y + \sigma_u)/2$.

As mentioned earlier, crack propagation in the composite was monitored *in-situ*. In addition, some of the tests were stopped at periodic increments of crack growth, were unloaded and the specimens transferred to a JEOL 35-CF scanning electron microscope. The unloading compliance was recorded as an additional measure of crack length while the crack path on the external surfaces was examined at high magnification. The fracture surfaces were also examined for all specimens using the SEM.

3. RESULTS

The tensile properties of both the unreinforced alloy and the composite are summarized in Table 1 for both the aging conditions studied, while Fig. 3 illustrates the TEM views of the microstructure of the UA and OA composites. The particular differences between the two conditions relates to the presence and type of aging particles at the SiC/matrix interfaces, grain boundaries and the matrix. Precipitate free zones (PFZ) were additionally observed near the grain boundaries and also at the SiC/matrix interfaces, while high resolution STEM analyses performed an a VG HB501 FEG/STEM to analyze the local chemistry in these regions are summarized elsewhere [18]. Figures 4–6 illustrate the effect of reinforcement volume fraction on the yield stress, ultimate tensile strength and elongation, respectively. The reduction in ductility with the addition of a brittle reinforcement to a ductile matrix is well documented [9]. Humphreys [9] has similarly observed a decrease in yield stress and UTS for particulate reinforced composites whose matrices consisted of a high strength aluminum alloy, such as the 7XXX series materials used presently. However, it should be noted that lower strength matrices often exhibit yield strengths in excess of that of the monolithic material [9]. As can clearly be seen from Figs 5 and 6, the uniaxial tensile properties are nearly the same for the UA and OA microstructures at a given reinforcement volume fraction. Further,

Table 1. Tensile properties of unreinforced and composite materials

Material	Yield stress (MPa)	Ultimate tensile strength (MPa)	Elongation (percent)
UA–unreinforced	509	638	20
UA—15% SiC	417	564	4.9
UA–20% SiC	381	502	4.3
OA–unreinforced	553	594	19
OA–15% SiC	427	588	3.5
OA–20% SiC	406	459	3.4

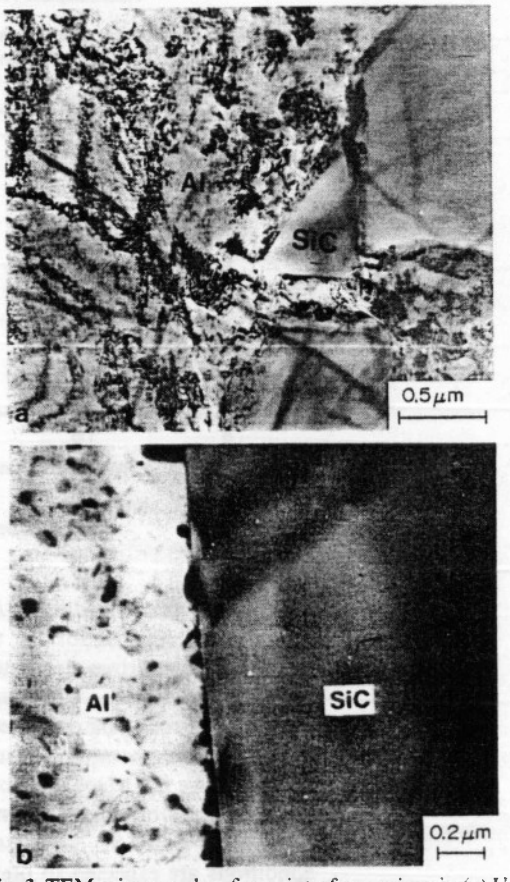

Fig. 3. TEM micrographs of near interface regions in (a) UA and (b) OA composites.

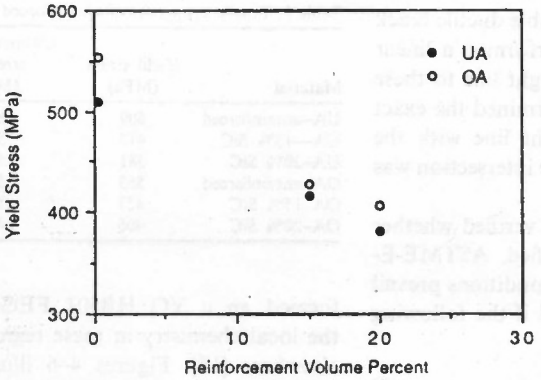

Fig. 4. Plot of yield stress as a function of vol.% SiC reinforcement.

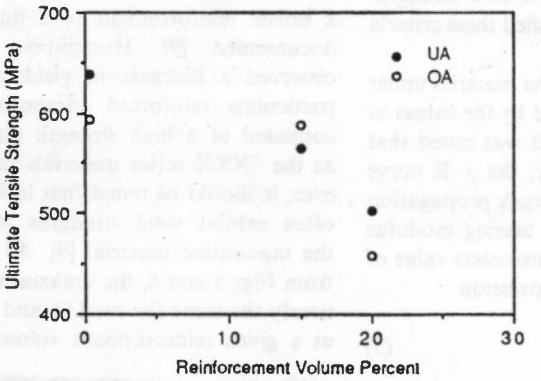

Fig. 5. Plot of ultimate tensile strength as a function of vol.% SiC reinforcement.

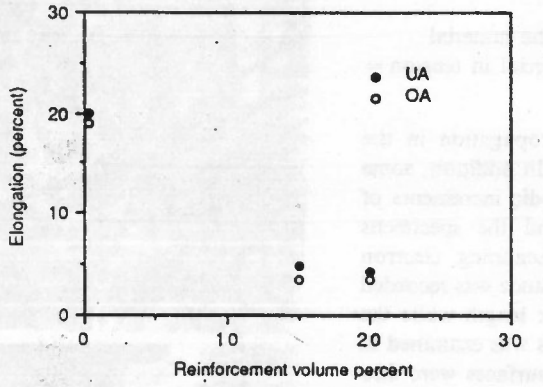

Fig. 6. Plot of elongation as a function of vol.% SiC reinforcement.

the matrix microhardness ($H_v = 140$, 30 g load) values were identical for the two aging conditions.

Table 2 summarizes J_{Ic} and tearing modulus values for both the unreinforced material and the composite for both matrix aging conditions (i.e. UA and OA). Although the composite and the unreinforced material were not tested at identical thicknesses, since the conditions of valid J measurement as prescribed by ASTM-E-813-81 were satisfied, plane strain conditions are expected to prevail in both cases and the J_{Ic} values deemed comparable. It is shown that the J_{Ic} values were nearly identical for the unreinforced materials, and that the tearing modulus of the OA unreinforced material is slightly higher than that of the UA material. Despite the similar crack initiation behavior of the UA and OA unreinforced materials, Figs 7 and 8 illustrate the dramatically different J-resistance curves obtained for UA and OA microstructures in the 15% SiC composite, while the effects of reinforcement volume fraction on J_{Ic} values are shown in Fig. 9. It can be seen that while the UA material exhibits a nearly linear decrease in J_{Ic} as the volume fraction of SiC increases from 0 to 20%, the OA material shows a much more rapid and non-linear decrease over the same range of volume fractions. Further, the J_{Ic} values for the OA composite are about 50% lower than those for the UA composite at the given volume fractions. The

Table 2. Fracture properties of unreinforced and composite materials

Material	J_{Ic} observed (kJ/m^2)	J_{Ic} predicted (kJ/m^2)	Tearing modulus
UA–unreinforced	31.0	—	6.0
UA–15% SiC	16.3	14.6	1.83
UA–20% SiC	11.7	12.1	1.84
OA–unreinforced	31.5	—	7.2
OA–15% SiC	7.4	14.9	0.74
OA–20% SiC	5.5	12.9	0.79

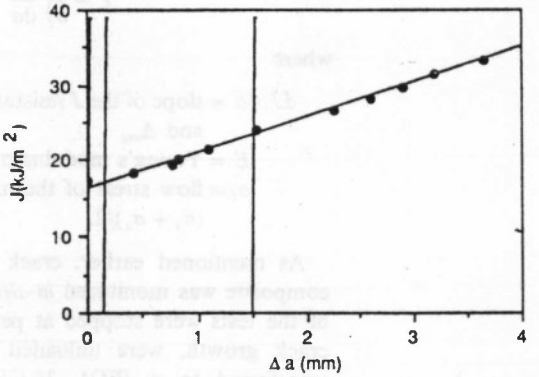

Fig. 7. Plot of the J–Δa curve for the 15% SiC reinforced UA composite. Exclusion lines shown. Blunting line obscured by vertical axis.

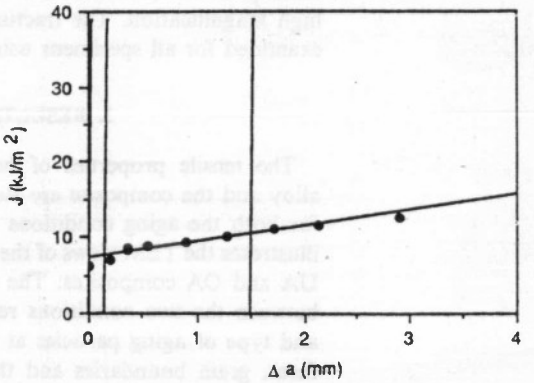

Fig. 8. Plot of the J–Δa curve for the 15% SiC reinforced OA composite. Exclusion lines shown. Blunting line obscured by vertical axis.

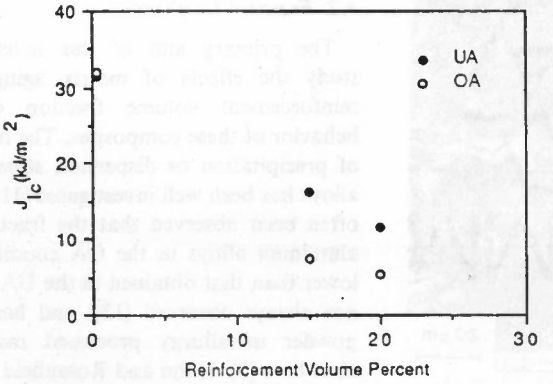

Fig. 9. Plot of J_{Ic} vs reinforcement volume fraction.

tearing modulus of the OA composite is also significantly lower than that of the UA composite, although these values appear to be independent of volume fraction in the range 15–20% reinforcement.

Although the fractographic details were not significantly different for the unreinforced materials, fracture mechanisms operative in the composite exhibited a strong dependence on the matrix aging condition. In the UA composite, fracture occurs predominantly by the fracture of SiC particulates. Matching surface fractographs taken in the UA condition reveals fractured SiC particles at the base of dimples, surrounded by ductile failure of the matrix as shown in Fig. 10.

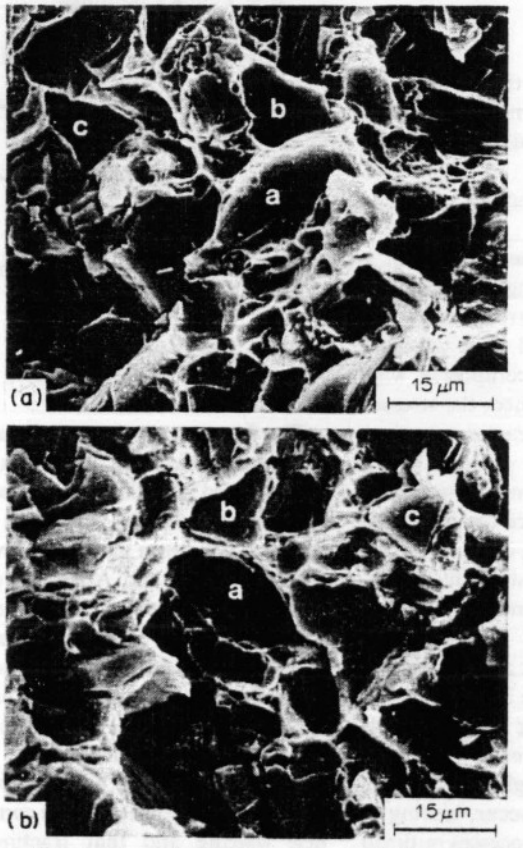

Fig. 10. Matching fractographs for the UA composite. Fractured SiC particles observed on both surfaces.

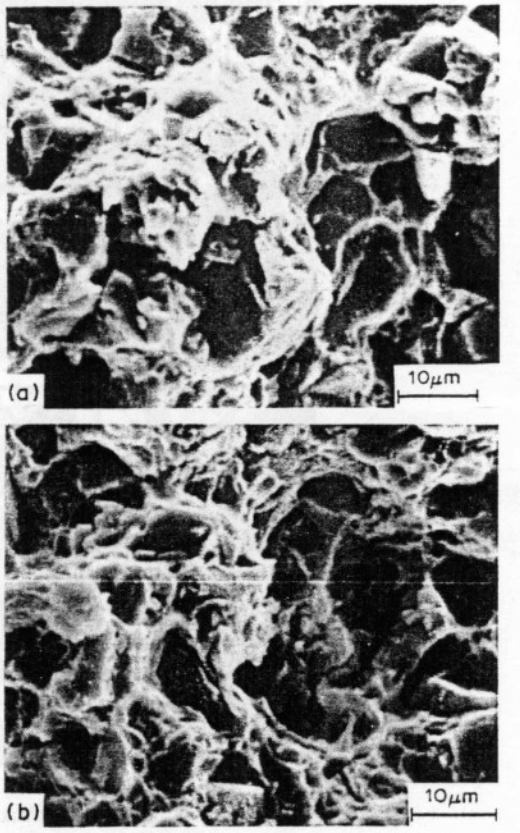

Fig. 11. Matching fractographs for the OA composite. Fracture near the SiC/matrix interface observed.

The area fraction of cracked SiC particles present on the fracture surface, determined using a Zeiss videoplan analyzer equipped with statistical software, was approximately 18%. In contrast, the fracture surfaces of the OA composites revealed considerably less failure of the SiC, with a fracture surface coverage by SiC of 11%. Matching surface fractographs revealed failure predominantly in the matrix and near the SiC/matrix interfaces as shown in Fig. 11. The crack tip regions in specimens unloaded after increments of crack growth are shown in Fig. 12 for the UA and OA composites. Fracture of the SiC was again observed for the UA composites, with failure near the SiC/matrix interfaces in the OA composite.

4. DISCUSSION

4.1. Tensile properties

The physical basis of the influence of particulate reinforcements on the strength of metal matrix composites is not well understood. One of the approaches is the modified shear lag theory [10] which derives its basis from fiber reinforced composites. It essentially involves the concept of a load transfer from the matrix to the fiber via the fiber interface [9]. However, as pointed out by Humphreys [9], as the fibers become shorter, modifications have to be made for the factors governing the load transfer from matrix to

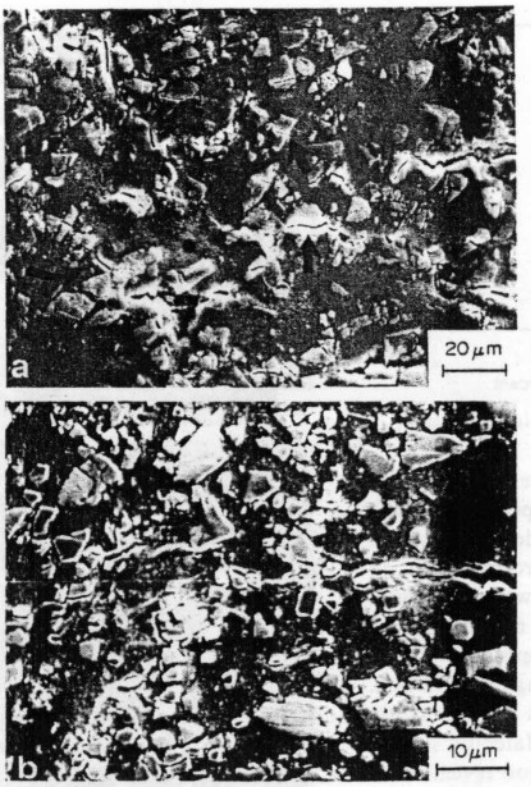

Fig. 12. Crack tip region in the (a) UA and (b) OA composites. Predominance of cracked particles in UA with failure near interfaces in OA.

fiber. Other factors contributing to the strength of a composite include thermal mismatch and associated dislocations. These models would in general lead to an improvement of the yield stress with the addition of a particulate reinforcement.

As observed by Humphreys [9], the addition of a brittle reinforcement in high strength aluminum alloys may even decrease the yield stress. Indeed in the present composite, this was found to be the case. One plausible explanation is that as composites with these high strength matrices are strained, the stresses on the reinforcement become large. Fracture can then occur in the reinforcement in the presence of a pre-existing flaw in the reinforcement, probably formed during earlier processing. Once the reinforcement fractures, the net load carrying capacity of the composite decreases and thus yield stress might decrease. It is also possible that the mismatch between reinforcement and matrix leads to a large stress concentration near the reinforcement and the matrix in that region fails prematurely, while loss of alloying elements (e.g. Mg) during processing may also contribute to these observations. In lower strength matrices, the stresses reached locally might not be large enough for either of these effects to occur, leading to strength improvement through the processes outlined earlier.

4.2. Fracture toughness

The primary aim of this investigation was to study the effects of matrix aging condition and reinforcement volume fraction on the fracture behavior of these composites. The fracture toughness of precipitation or dispersion strengthed aluminum alloys has been well investigated [11, 12]. While it has often been observed that the fracture toughness of aluminum alloys in the OA condition is somewhat lower than that obtained in the UA condition, this is not always observed [13], and has been shown in powder metallurgy processed materials discussed elsewhere [3]. Hahn and Rosenfield [14] analyzed the toughness data obtained by a variety of investigators on a number of aluminum alloys. In accordance with the model proposed by Rice and Johnson [15], they assumed that crack extension would proceed when the extent of heavily deformed region ahead of the crack tip is comparable to the width of the unbroken ligaments separating cracked particles. Further, they showed that under these conditions, the stress intensity factor could be related to the volume fraction of reinforcement through the relation

$$K_{Ic} = [2\sigma_Y E(\pi/6)^{1/3} D]^{1/2} f_v^{-1/6} \quad (4)$$

where

K_{Ic} = critical mode I stress intensity factor
σ_Y = yield stress
E = Young's modulus
D = particle diameter
f_v = reinforcement volume fraction.

For plane strain conditions, such an equation can be rewritten in terms of J_{Ic} as

$$J_{Ic} = 2\sigma_Y (\pi/6)^{1/3} D(1-\nu^2) f_v^{-1/6} \quad (5)$$

where

J_{Ic} = critical mode I J integral
ν = Poissons ratio.

Hahn and Rosenfield found that a number of alloys satisfied this relationship within an error of 30%.

The fracture toughness of pure aluminum based particulate reinforced metal–matrix composites has been studied by Flom and Arsenault [1] while the behavior of Al–Mg–Cu based composites in the annealed condition have been investigated by Kamat *et al.* [2]. Flom and Arsenault concluded that submicron oxide particles, inclusions etc. are responsible for the microvoid coalescence mechanisms of fracture in the SiC/Al composites they studied [1] and indicated that with the above assumption their results agreed with a model similar to that of Hahn and Rosenfield [14]. Kamat *et al.* [2] concluded that fracture is controlled by the development of a dislocation cell structure of a size comparable to interparticle spacing and that fracture occurs by Al_2O_3 fracture. Their stress intensity values, at least for

small sizes of Al_2O_3 and lower volume fractions, were comparable with a Rice and Johnson [15] type model.

In the present investigation, it was found that the critical J integral value is not only a function of reinforcement volume fraction but also is a strong function of matrix aging condition. Table 2 summarizes the observed J_{Ic} values as well as those calculated using equation (4) based on Hahn and Rosenfield's model. It can be seen that the magnitude of the predicted values are acceptable for the UA composite but are considerable overestimations for the OA composite. Thus, the local fracture micromechanisms appear to play an important role in determining macroscopic fracture properties. In this composite, fracture property predictions based solely on the basis of uniaxial properties might be an oversimplification.

It should also be pointed out that the values of the J integral scale inversely with increases in volume fraction from 15–20%. It is thus possible that the fracture properties of these composites can be estimated using an energy based approach as a sum of the energy to fracture the matrix and the energy required to fracture the SiC or decohere the SiC/matrix interface. However, if one were to estimate the J_{Ic} values of the unreinforced material based on an extrapolation of the J_{Ic} values of the composites, a value of 30.1 kJ/m^2 and 13.1 kJ/m^2 would be obtained for the UA and OA conditions respectively. While the extrapolated value for the UA unreinforced material is close to the observed value of 31.5 kJ/m^2, the value for the OA material is much lower than the observed value of 32.0 kJ/m^2. Further, it can be seen that the initiation J values are nearly the same for the unreinforced material for both aging conditions. This would also indicate that the reinforcement/matrix interfaces in the OA materials provide lower energy sources for void initiation than they do in the UA material where SiC particle cracking predominates.

The above observations on the differences in energy required to crack the SiC or fracture near the SiC/matrix interface can be related to the differences in the microstructures between the UA and OA conditions at or near the interface. Recent high resolution STEM results [18] indicate that the segregation and precipitation in the UA material is very different from that in the PFZ at the interface in the OA material. The precipitates and segregation apparently contribute to the lowering of the local fracture energy by either directly weakening the interfacial bonding or by leading to depletion of solute near the interface, thereby leading to a weaker region adjacent to the interface. A TEM foil taken from a region directly below or ahead of a propagating crack in an OA material is shown in Fig. 13. The voids formed near the interface are localized to the near interface region in the OA composites.

The tearing modulus values seem to be relatively independent of the reinforcement volume fraction but

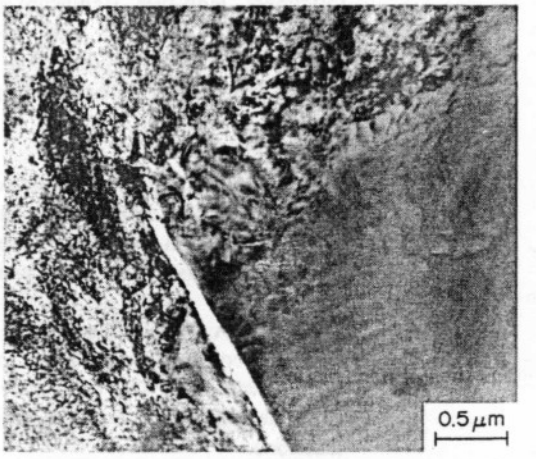

Fig. 13. TEM foil taken below fracture surface showing void formation near SiC/interface in the OA composite.

strongly dependent on matrix aging condition. The relative independence to volume fraction might be due to the small changes in volume fraction studied. As noted by Ritchie and Thompson [16], changes in microstructure can produce markedly different changes in crack initiation and growth characteristics. It should also be noted that the absolute value of dJ/da, the slope of the J–R curve, decreases as the volume fraction of reinforcement is increased. However, the decrease in flow stress associated with an increase in reinforcement volume fraction in this composite compensates for this decrease in dJ/da and the normalized tearing moduli are equal. The tearing moduli are, however, strongly dependent on matrix aging condition. As with the initiation toughnesses, the tearing modulus of the OA composite is less than 50% of the UA composite. Once again, this observation indicates that the relative energies of local fracture mechanisms must be taken into account in any analysis of the macroscopic crack growth toughness. While the fracture initiation toughness in the monolithic alloy were not significantly affected by these changes in microstructure, both fracture initiation and growth toughnesses were significantly affected by these changes in microstructure in these composites. Work is continuing using composites based on other aluminum alloy matrices to determine the generality of the observations and concepts reported presently [17].

5. CONCLUSIONS

The effects of systematic changes in microstructure, at equivalent yield stress and matrix microhardness were determined for an unreinforced and a SiC particulate reinforced Al–Zn–Mg–Cu aluminum alloy. The unreinforced alloy exhibited no measurable effect of aging condition on fracture initiation toughness and only a marginal effect on crack growth

toughness. However, significant differences in both the fracture initiation and growth toughnesses were obtained for the composite when tested under similar conditions. The following summarizes our findings:

1. While UA and OA composites exhibited similar tensile properties at identical volume fractions, the fracture initiation toughness (as measured by J_{Ic}) of the UA composite was about twice that of the OA composite.

2. The UA composite exhibited a linear decrease in J_{Ic} as the volume fraction of SiC was increased from 0–20% while the OA composite exhibited a more rapid decrease in J_{Ic} over the same range of volume fractions.

3. The crack growth toughness (as measured by the tearing modulus) of the UA composite was also about twice that measured for the OA composite.

4. Associated with this decrease in the crack initiation and growth toughnesses in going from a UA to a OA microstructure was a transition in the local fracture mode from SiC fracture (UA) to failure near the SiC/matrix interface (OA).

Acknowledgements—The authors would like to thank C. Liu for assistance with TEM and M. Strangwood, HARWELL, for the STEM analyses, as well as W. Hunt Jr of ALCOA for supply of the material. This work was partially supported by the U.S. Army Research Office (JJL) and by NASA NAGW 1193 (MM, JJL). Collaborative work with M. Strangwood is being supported by a N.A.T.O. Collaborative Grant.

REFERENCES

1. Y. Flom and R. I. Arsenault, *Acta metall.* 37, 2413 (1989).
2. S. V. Kamat, J. P. Hirth and R. Mehrabian, *Acta metall.* 37, 2395 (1989).
3. J. J. Lewandowski, C. Liu and W. H. Hunt Jr, In *Powder Metallurgy Composites* (edited by M. Kumar *et al.*), p. 117. TMS-AIME, Warrendale, Pa (1988).
4. J. J. Lewandowski, C. Liu and W. H. Hunt Jr, *Mater. Sci. Engng* A107, 241 (1989).
5. *ASTM Annual Book of Standards*, Am. Soc. Test. Mater., E-813, 713, (1987).
6. P. Doig and K. R. Abbott, *J. Test. Eval.* 12, 297 (1984).
7. M. Manoharan and J. J. Lewandowski, *Int. J. Fract.* 40, R34 (1989).
8. P. C. Paris, H. Tada, A. Zahoor and E. Ernst, ASTM STP 668, Am. Soc. Test. Mater. 5, (1979).
9. F. J. Humphreys, in *Mechanical and Physical Behavior of Metallic and Ceramic Composites* (edited by S. I. Anderson *et al.*), p. 51. Risø Natn. Lab., Denmark (1988).
10. V. C. Nardone and K. M. Prewo, *Scripta metall.* 20, 43 (1986).
11. C. Q. Chen and J. F. Knott, *Metal Sci.* 15, 357 (1981).
12. G. G. Garrett and J. F. Knott, *Metall. Trans. A* 9A, 1187 (1978).
13. J. T. Staley, in *10th Symp. on Naval Structural Mechanics—Fracture Mechanics*, Univ. of Virginia. p. 671 (1978).
14. G. T. Hahn and A. R. Rosenfield, *Metall. Trans A* 6A, 653 (1975).
15. J. R. Rice and M. A. Johnson, *Inelastic Behavior of Solids* (edited by M. F. Kaninen *et al.*), p. 641. McGraw-Hill, New York (1969).
16. R. O. Ritchie and A. W. Thompson, *Metall. Trans. A* 16A, 233 (1985).
17. M. Manoharan and J. J. Lewandowski, *Scripta metall.* 23, 301 (1989).
18. M. Strangwood, C. A. Hippsley and J. J. Lewandowski, *Scripta metall. mater.* To be published.

JOURNAL OF MATERIALS SCIENCE LETTERS 10 (1991) 461–463

Laminated composites with improved bend ductility and toughness

L. YOST ELLIS, J. J. LEWANDOWSKI
Department of Materials Science and Engineering, Case Western Reserve University, Cleveland, OH 44106, USA

Metal-matrix composites are being considered for a range of structural and non-structrual applications because of their high specific stiffness and strength [1], in addition to the possibility of a reduced coefficient of thermal expansion. Despite these advantageous properties, reduced ductility and lower energy-absorbing capabilities [2, 3] are often obtained in many metal-based composites in comparison with the monolithic materials. Recent reviews have presented the effects of various microstructural features on the fracture of particulate-reinforced metal-matrix composites [1–7]. However, a potential way of increasing the energy-absorbing capabilites of such materials is to incorporate one or more ductile layers into the composite piece, as has been demonstrated elsewhere with metal-matrix composites [3, 8] and in the ductile phase toughening of brittle matrix materials [9, 10].

In this study laminated specimens were fabricated via co-extrusion to investigate the effects of a laminated structure on smooth bend properties. The composite material utilized was a 2××× series (wt %:3.5 Cu, 1.5 Mg, 0.4 Zr, 0.21 Mn, balance Al) aluminium matrix, designated MB-85, reinforced with 15 vol % SiC particulates (average size 13 mm) and the ductile layer was nominally a 6061 aluminium. The composite and aluminium layers were bonded via co-extrusion at 370 °C. Bend bars measuring 10 mm in total width and with the thickness of the aluminium layer ranging from 0 to 4 mm were subsequently machined as shown in Fig. 1. Testing was conducted on the specimens in the "O" temper under displacement control with a crosshead speed of 0.5 mm min^{-1} on an Instron 1125 universal testing machine. The laminated specimens were tested such that the ductile layer was loaded in tension. The load, total displacement (load point) and area under the curve were recorded.

The laminated specimens exhibited an increase in the bend ductility over the 100% composite specimens, and the appearance of the load–displacement traces obtained were dependent on the thickness of the aluminium layer. Fig. 2 presents the load–displacement traces for a 100% composite specimen and that for a laminated specimen containing a 0.8 mm layer of aluminium tested in four-point bending. The y-axis plots the normalized load, which represents the applied load divided by the depth of the specimen. Although both specimens failed catastrophically upon reaching some maximum load, the total load point displacement for the laminate is twice that of the 100% composite bar, indicating that a thin layer of ductile material on the tensile surface can significantly increase the bend ductility. Furthermore, as the maximum load attained in the laminate slightly exceeds that of the 100% composite specimen, it is clear that the total energy absorbed (i.e. the area under the curve) is greater for the laminate.

Increasing the thickness of the aluminium layer to 1.5 mm and testing in three-point bending produces the load-displacement trace shown in Fig. 3. Fig. 3 shows that the load drop at point A is followed by an increase in load to point B, where a large drop occurs to point C, followed by a continuously dropping load with increased displacement. Examination of a similar specimen unloaded at an earlier stage in the load–displacement trace illustrates the "source" of the load drop at point A, as shown in Fig. 4. A non-catastrophic cracking initiated in the composite near the interface between the composite and monolithic layers, thereby producing the first load drop. As the load increased to point B, the crack grew in a stable manner away from the interface and extended in the composite layer. The

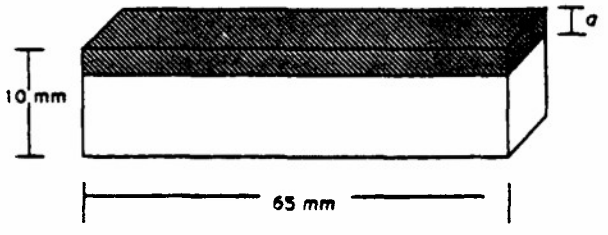

Figure 1 Schematic of the bend specimen. (■) Aluminium and (□) composite. $0 < a < 4$ mm.

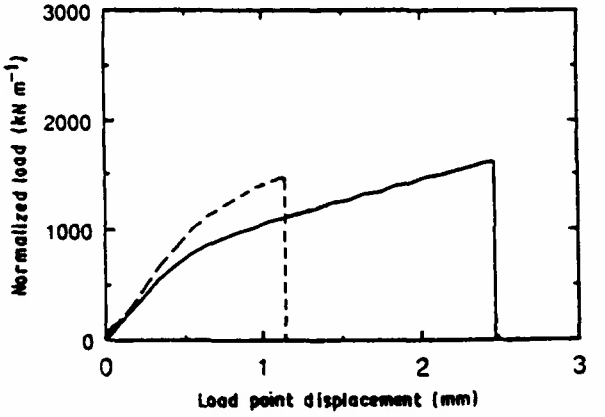

Figure 2 Load–load point displacement trace for (——) laminate with a 0.8 mm layer of aluminium and (– – –) a 100% composite specimen.

0261-8028/91 $03.00 + .12

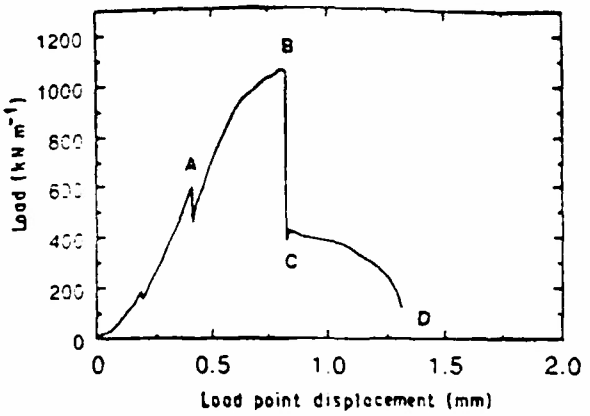

Figure 3 Load–load displacement trace for laminate with a 1.5 mm layer of aluminium.

Figure 4 Side view of bend bar illustrating the aluminium–composite interface after unloading. A crack has initiated in the composite near the aluminium–composite interface. Deformation within the aluminium (arrow), near the crack tip, is apparent.

aluminium layer was completely intact during this stable cracking although intense local deformation was observed in the aluminium layer, shortly after the crack initiation, as indicated in Fig. 4. However, the aluminium layer began to neck as the crack in the composite advanced, between points A and B. The aluminium failed catastrophically at point B, resulting in the large load drop from B to C. Stable crack propagation continued to occur in the composite layer from point C onward. Fig. 5 shows a specimen unloaded at point D and illustrates the extreme deformation and necking in the aluminium layer.

Consitent with the above description, the fracture surface of the failed laminate specimens shows a

Figure 5 Laminate containing 1.5 mm thick layer of aluminium unloading at point D in Fig 3. Significant necking of the aluminium layer is evident.

region of intense shear at the interface between the composite and monolithic layer (Fig. 6). The region of intense shear lies predominantly within the aluminium layer. Dimpled fracture is observed in each of the layers of the laminate.

In conclusion, the present results illustrate the benefits to the bend ductility obtained by the addition of a ductile layer to the tensile surface of particulate-reinforced metal-matrix composites tested in bending. This is accomplished without significantly decreasing the load-carrying capacity of the bar, thereby increasing the energy-absorbing capacity. Laminated specimens may also be designed such that the crack will propagate in a stable

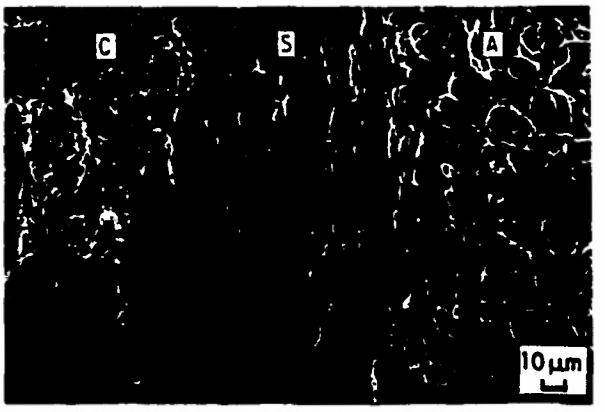

Figure 6 Scanning electron microscopic view of laminate taken at the aluminium–composite interface. A region of shear deformation (S) lies in the aluminium between the fracture surfaces of the composite (C) and aluminium (A) layers.

manner, thereby avoiding catastrophic failure, as shown elsewhere [7, 8, 11]. Continuing work will focus on the effects of changes in the laminate structure, thickness and heat treatment on the resultant properties.

Acknowledgement

This work was supported by the US Army Research Office (L.Y.E, J.J.L).

References

1. J. J. LEWANDOWSKI, *SAMPE Q.* **20** (1989) 33.
2. J. J. LEWANDOWSKI, C. LIU and W. H. HUNT, Jr, in "Processing and properties of powder metallurgy composites", edited by P. Kumar, K. Vedula and A. Ritler (TMS–AIME, Warrendale, Pennsylvania, 1988) p. 117.
3. *Idem*, *Mater. Sci. Engng.* **A107** (1989) 241.
4. M. MANOHARAN, C. LIU and J. J. LEWANDOWSKI, in 7th International Conference on Fracture, edited by K. Salama, K. Ravi-Chander, D. M. R. Taplin and P. Rama Rao (Pergamon Press, Oxford, 1989) p. 2977.
5. S. V. KAMAT, J. P. HIRTH and R. MEHREBIAN, *Acta Metall.* **37** (1989) 2395.
6. M. MANOHARAN and J. J. LEWANDOWSKI, *ibid.* **38** (1990) 489.
7. J. J. LEWANDOWSKI, in Proceedings of the 2nd International Ceramics and Composites Conference, edited by M. D. Sacks, (The American Ceramic Society, Westerville, OH).
8. M. MANOHARAN, L. Y. ELLIS and J. J. LEWANDOWSKI, *Scripta Metall.* **24** (1990) 1515.
9. V. KRSTIC, P. NICHOLSON and R. HOAGLAND, *J. Amer. Ceram. Soc.* **64** (1981) 449.
10. M. F. ASHBY, F. J. BLUNT and M. BANNISTER, *Acta Metall.* **37** (1989) 499.
11. L. Y. ELLIS and J. J. LEWANDOWSKI, unpublished work.

Received 4 September
and accepted 8 October 1990

Scripta METALLURGICA et MATERIALIA
Vol. 24, pp. 1515-1519, 1990
Printed in the U.S.A.
Pergamon Press plc

LAMINATED COMPOSITES WITH IMPROVED TOUGHNESS

M. Manoharan, L. Ellis and J.J. Lewandowski
Department of Materials Science and Engineering
Case Western Reserve University
Cleveland, Ohio - 44106

(Received May 18, 1990)
(Revised May 30, 1990)

Introduction

Metal-matrix composites are emerging as an important class of materials in the continuing quest for improved strength, stiffness and other desirable properties. Reinforcing a ductile, tough metal with a strong ceramic is one method of achieving such an improvement in properties. Discontinuous reinforcements such as particulates or whiskers tend to produce composites with a greater degree of isotropy in properties compared to continuous fiber reinforcements. Further, if the metallic matrix is age hardenable, suitable heat treatments can be devised to optimize properties (1,2). The flaw tolerance of metal-matrix composites is important when these materials are to be used as structural components.

The effects of reinforcement size and volume fraction on the fracture properties of composites based on various aluminum alloys (1-9) have been investigated. Most of these investigations have focussed on the fracture initiation properties of these composites while a few (7-9) have also studied the crack growth toughness . It has generally been found that the brittle reinforcement tends to decrease both the initiation and growth toughnesses, although the effect of reinforcement on decreasing the growth toughness seems to be more pronounced (8,9). One of the ways of improving the toughness would be to manufacture laminated composites incorporating either one or more ductile/tough layers which would retard the process of crack growth. These layers could be formed by various processes and can consist of the same matrix alloy or other aluminum alloys. Such layered composites were used by Lewandowski et. al. (1,10) to study the crack propagation in an aluminum composite. They found that the retarding effect of the ductile backing layer was sufficient to allow the in-situ monitoring of the micromechanical events of fracture. The present investigation uses a similar design to quantitatively evaluate the enhancement in initiation and growth toughness in an aluminum composite reinforced with particulate SiC and represents part of our continuing work on increasing the toughness of metal-matrix composites (11).

Experimental Procedures

The composite studied in the present investigation was a powder metallurgy 2XXX series alloy, designated MB-85 containing in wt. % : 3.5 Cu, 1.5 Mg, 0.4 Zr, 0.21 Mn, Bal Al reinforced with 15 volume percent silicon carbide particulate (average size 13 μ m). Heat treatments consisted of a solution treatment at 495^{0}C/4 hours, followed by a cold water quench and artificial aging at 190^{0}C/3 hours to produce a composite in the underaged condition. The backing material used in the laminated specimen, described in the next paragraph, was nominally a 6061 aluminum alloy.

The initiation and growth toughnesses of the composite and the monolithic 6061 alloy were tested using a compact tension specimen geometry, as shown in Fig. 1. The effect of the ductile backing on retarding crack propagation was studied using the laminated design shown in Fig. 2 (2,10). The proportion of the 6061 alloy thickness in the laminated specimen was about 25%. All of the compact tension specimens had identical crack lengths and a/W ratios to ensure similitude.

Fracture properties were evaluated in general accordance with the standard procedure for J testing, ASTM E-813-81 (12). A precrack of nominal root radius 30 μm was introduced using an electron discharge machining process. Our earlier work (13) had shown that plane strain fracture toughness results obtained using this notch root radius were equivalent to the results using a fatigue precrack for a similar composite. The crack was followed optically using a travelling microscope fitted to a stage equipped with a LVDT. For this purpose, the external surfaces of the specimens were polished metallographically, and the details of crack propagation were studied in-situ with the use of a high power optical microscope connected to a video recording system.

0036-9748/90 $3.00 + .00

The fracture toughness testing was carried out on a MTS servo-hydraulic test system operated under stroke control at a crosshead speed of 25 μ m/minute. Displacement was measured across the crack mouth using a clip-gage. The load, displacement and crack length data were continuously input and stored in a computer.

J was calculated using the equation,

$$J = \frac{A}{Bb} f(a_0/W) \tag{1}$$

where,

A = area under the load-displacement record.

B = specimen thickness.

b = initial uncracked ligament

a_0 = original crack size including fatigue precrack.

$f(a_0/W)$ = a geometry dependent constant, from ASTM-E-813-81.

The standard procedure for plane strain J - Integral estimation, ASTM E-813-81, was followed for the construction of the J resistance curve. This procedure involves the assumption that the blunting behavior followed the relation, $J = 2\sigma_f \Delta a$, where the flow stress σ_f was set equal to $(\sigma_y + \sigma_u)/2$. The exclusion lines were then drawn at offsets of 0.15 mm and 1.5 mm, respectively, parallel to the blunting line. The points that lie within these exclusion lines represent valid data points as they correspond to stable ductile crack extension. A computer program performed a linear regression analysis and fitted a straight line to these data points. The program then determined the exact point of intersection of this straight line with the blunting line and the value of J at the intersection was taken as J_{Q_c}.

Once J_{Q_c} is determined, it can be verified whether conditions of plane strain are satisfied. ASTM-E-813-81 prescribes that plane strain conditions prevail and a valid J_{I_c} has been obtained if the following conditions are satisfied,

$$B, b > 25 J_{I_c}/\sigma_f \tag{2}$$

where B is the net thickness, b is the uncracked ligament length and σ_f is the effective flow strength. All tests conducted in this study satisfied these criteria for valid J measurement.

The crack initiation behavior of the material under these conditions is thus characterized by the values of J_{I_c}. In addition to determining J_{I_c} it was noted that in all the tests conducted presently, the J-R curve had a non-zero positive slope. The crack propagation behavior was characterized by the tearing modulus concept of Paris et al (9). The dimensionless value of tearing modulus is given by the expression,

$$T = \frac{E}{\sigma_f^2} \frac{dJ}{da} \tag{3}$$

where

dJ/da = Slope of the J resistance curve between Δ_c and Δ_{max}

E = Young's modulus of the material

σ_f = Flow stress of the material in tension = $(\sigma_y + \sigma_u)/2$

As mentioned earlier, crack propagation in the composite was monitored in-situ. The fracture surfaces were also examined for all specimens using the SEM.

Results and Discussion

Figs 3 and 4 summarize the J-R curves for both the composite and the laminated specimens. The J_{I_c} value of the 'pure' composite is 8 kJ/m^2 while that of the laminated composite is 9 kJ/m^2. It can be seen that the crack initiation toughness of the composite is enhanced by about 10% by the addition of a realtively thin ductile layer. It should be noted that the 6061 backing material used in this case has only a moderate fracture toughness ($J_{I_c} = 17 kJ/m^2$), as obtained in thicker specimens tested elsewhere (15). Using backing material with higher fracture toughness should enhance the initation value even further (11).

The growth toughness of the composite, as measured by the slope of the J-R line or by the tearing modulus, is dramatically enhanced by the addition of this thin backing layer. The enhancement in the tearing modulus exceeds 250%, increasing from about 0.9 for the 'pure' composite to about 2.5 for the laminate. The tearing modulus was calculated using composite values for E and σ_f in both cases, while the crack length was measured on the composite face of the layered specimen, farthest away from the ductile backing. Thus the crack length is conservatively measured in this experiment and the net enhancement in overall crack growth should be even greater. This ability to improve the crack growth toughness by a large amount is important when these materials are to be used in structures where the growth of a flaw, once initiated, has to be controlled. This enhancement in the crack growth toughness is achieved because more energy is required to initiate and propagate a crack in the 6061 backing in comparision to the composite as originally proposed (1,10). Thus one can take advantage of the enhancement in stiffness and strength offered by the incorporation of a very strong reinforcement without overly sacrificing the flaw tolerant nature of aluminum alloys. Additional work is focussing on the effects of different backing materials in an attempt to produce additional increases in both initiation and growth toughnesses.

Acknowledgements

This work was supported by the U.S. Army Research Office (MM, LE, JJL) with partial support from NSF-DMR-89-58326 (JJL).

References

1. J.J. Lewandowski, C. Liu and W.H. Hunt Jr., in 'Processing and Properties of Powder Metallurgy Composites', M. Kumar et. al. eds, TMS-AIME, Warrendale, PA, 117, (1988).
2. J.J. Lewandowski, C. Liu and W.H. Hunt Jr., Mat. Sci. Engr., A107 , 241, (1989).
3. M. Manoharan, C. Liu and J.J. Lewandowski, in International Conference on Fracture, K. Salama et. al. eds., Pergamon, 2977, (1989).
4. S.V. Kamat, J.P. Hirth and R. Mehrabian, Acta Metall., 37 , 2395, (1989).
5. M. Manoharan and J.J. Lewandowski, Scripta Metall., 23 , 1801, (1989).
6. Y. Flom and R.J. Arsenault, Acta Metall., 37 , 2413, (1989).
7. M. Manoharan and J.J. Lewandowski, Acta. Met., in review.
8. M. Manoharan and J.J. Lewandowski, Acta. Met., 38 , 489, (1990).
9. M. Manoharan and J.J. Lewandowski, Scripta Metall., 23 , 301, (1989).
10. J.J. Lewandowski and C. Liu, Presented at the TMS-AIME Meeting, Denver, Feb. 23-26, (1987).
11. L.Ellis, M. Manoharan and J.J. Lewandowski, Unpublished research.
12. ASTM Annual Book of Standards, Am. Soc. Test. Mat., E-813, 713, (1987).
13. M. Manoharan and J.J. Lewandowski, Int. J. Frac., 40 , R34, (1989).
14. P.C. Paris, H. Tada, A. Zahoor and H. Ernst, ASTM STP 668, Am. Soc. Test. Mat., 5, (1979).
15. M. Manoharan and J.J. Lewandowski, Unpublished Research.

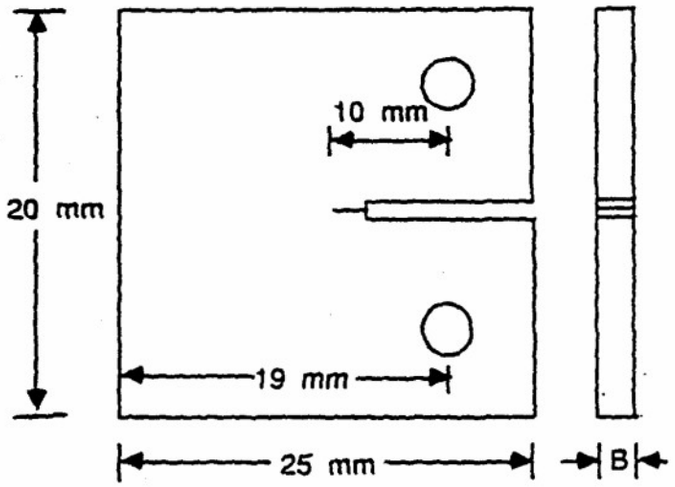

B (Composite) = 2.5 mm
B (Laminate) = 5.0 mm

Fig. 1 Schematic of Compact Tension Specimen.

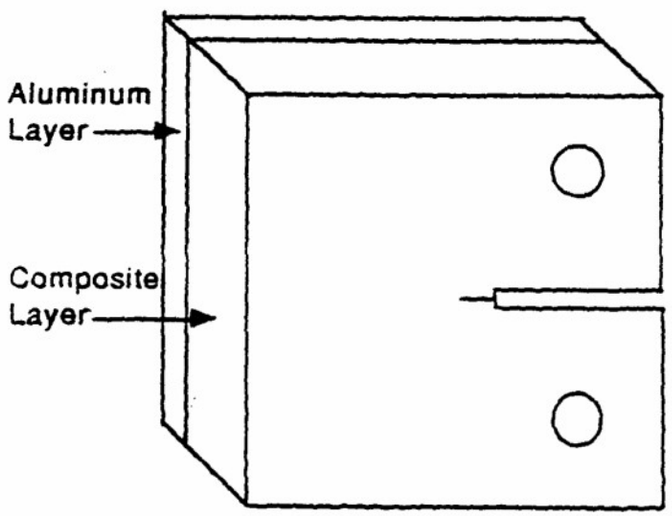

Fig 2. Design of the Laminate Specimen (2,10).

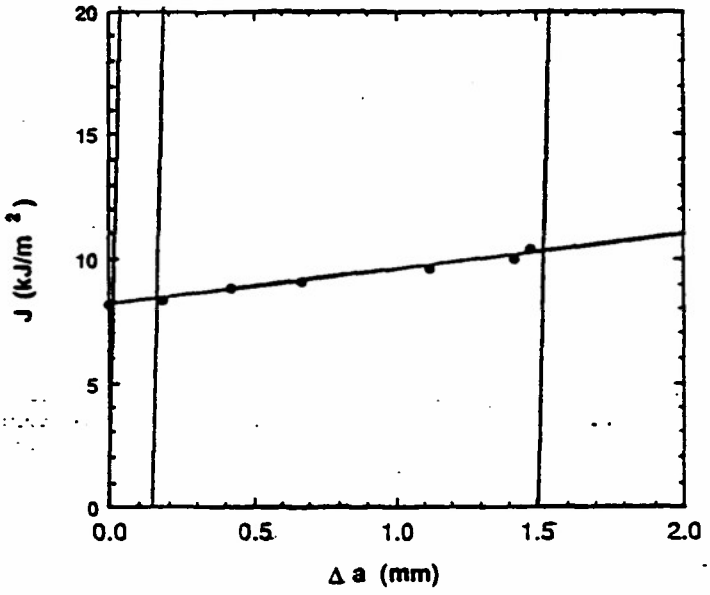

Fig. 3 Plot of J vs. Crack Length for the Composite.

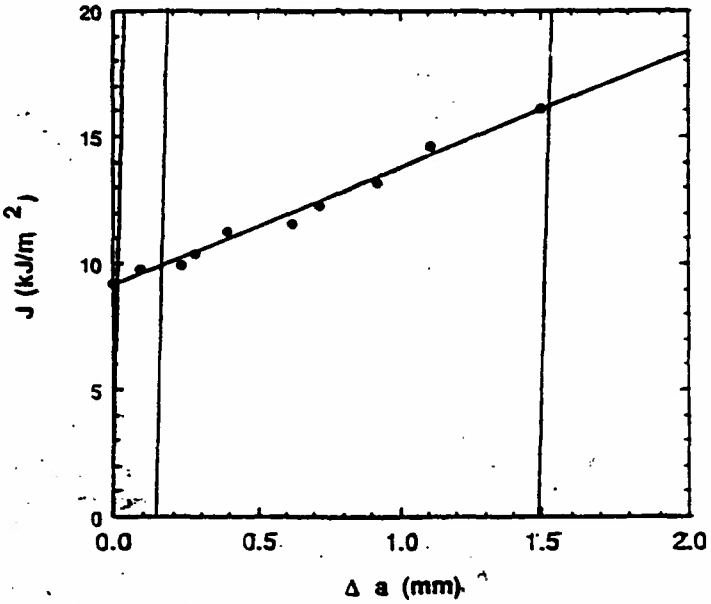

FIG. 4 Plot of J vs. Crack Length for the Laminate.

8 Joule, J. P. 1859. "On Some Thermo-Dynamic Properties of Solids," *Philos. Trans. R. Soc.*, 149: 91-131.

9 Compton, K. T. and D. B. Webster. 1915. "Temperature Changes Accompanying the Adiabatic Compression of Steel," *Phys. Rev.*, 5(Series 2):159-168.

10 Dillon, O. W. and T. R. Tauchert. 1966. "The Experimental Technique for Observing the Temperature Due to the Coupled Thermoelastic Effect," *Int. J. Solids Str.*, 2:385-390.

11 Belgen, M. H. 1967. "Structural Stress Measurements with an Infrared Radiometer," *ISA Trans.*, 6:49-53.

12 Stanley, P. and W. K. Chan. 1985. "Quantitative Stress Analysis by Means of the Thermoelastic Effect," *J. Strain Anal.*, 20:129-137.

13 Gilmour, I. W., A. Trainor and R. N. Haward. 1978. "The Thermoelastic Effect in Glassy Polymers," *J. Polym. Sci.: Polym. Phys. Ed.*, 16:1277-1290.

14 Haward, R. N. and A. Trainor. 1974. "The Thermoelastic Effect in PMMA," *J. Mater. Sci.*, 9:1243-1254.

15 Jordan, E. H. and B. I. Sandor. 1978. "Stress Analysis from Temperature Data," *J. Testing and Eval., JTEVA*, 6:325-331.

16 Stanley, P. and W. K. Chan. 1986. "SPATE Stress Studies of Plates and Rings under In-Plane Loading," *Exper. Mech.*, 26:360-370.

17 Higuchi, M. and Y. Imai. 1970. "Rheological Interpretation of Heat Generation Associated with Fatigue of Polycarbonate," *J. Appl. Polym. Sci.*, 14:2377-2383.

18 Nowacki, W. 1975. *Dynamic Problems of Thermoelasticity*. Noordhoff.

19 Thomson, W. 1857. "On the Thermo-Elastic and Thermo-Magnetic Properties of Matter," *Q. J. Math.*, 1:57-77.

20 Jones, R. M. 1975. *Mechanics of Composite Materials*. Washington, DC: Scripta.

21 Timoshenko, S. P. and J. N. Goodier. 1970. *Theory of Elasticity, 3rd Ed.* New York: McGraw-Hill.

22 Oliver, D. E. 1987. "Stress Pattern Analysis by Thermal Emission," Chapter 14 in *SEM Handbook on Experimental Mechanics*, A. S. Kobayashi, ed., Prentice-Hall.

23 Bakis, C. E. and K. L. Reifsnider. 1989. "Adiabatic Thermoelastic Measurements," Section VII B in *SEM Manual on Experimental Methods for Mechanical Testing of Composites*, R. L. Pendleton and M. E. Tuttle, eds., *Soc. Exp. Mech.*, pp. 139-146.

24 Chamis, C. C. 1984. "Simplified Composite Micromechanics Equations for Hygral, Thermal, and Mechanical Properties," *SAMPE Q.*, 15:14-23.

25 Kriz, R. D. and W. W. Stinchcomb. 1982. "Effects of Moisture, Residual Thermal Curing Stresses, and Mechanical Load on the Damage Development in Quasi-Isotropic Laminates," in *Damage in Composite Materials, STP 775*, K. L. Reifsnider, ed., Philadelphia: ASTM, pp. 63-80.

Combined Mode I–Mode III Fracture Toughness of a Particulate Reinforced Metal–Matrix Composite

M. MANOHARAN[1] AND J. J. LEWANDOWSKI[2]
Department of Materials Science and Engineering
Case Western Reserve University
Cleveland, OH 44106

(Received November 13, 1989)
(Revised April 2, 1990)

ABSTRACT: The aim of this investigation was to determine the fracture behavior of a particulate reinforced aluminum alloy composite under combined mode I–mode III loading conditions. A modified three point bend specimen was used to carry out these tests. It was found that the mode I loading condition was energetically most favorable. Addition of mode III components to the system seems to increase the amount of redundant work during fracture without affecting the critical fracture criterion.

KEY WORDS: aluminum composite, metal–matrix composite, combined mode fracture, mode I–mode III fracture.

I. INTRODUCTION

MOST OF THE work in the field of fracture mechanics has been concentrated on the study of fracture under mode I (i.e., tensile mode) loading conditions. However, many structures are loaded in complex patterns and the cracks in them are subjected to various combinations of the three possible loading modes, mode I (tension), mode II (shear) and mode III (transverse shear).

There has been a limited amount of experimental work done on mixed mode fracture. The observations on combined mode I–mode III fracture have been very scarce and there is no general agreement among authors on the effect of the addition of a mode III component to pure mode I loading. Although the general conclusion is that the addition of mode III lowers the mode I contributions [1,2], Pook [3] found the mode I toughness to be relatively insensitive to transverse shear. Rosenfield and Duckworth [4] as well as Suresh and Tschegg [5] studied more brittle materials. While the former workers [4] found the mode I toughness

[1]Research Associate.
[2]Associate Professor.

0021-9983/91/07 0831-11 $6.00/0

to be independent of the mode III component the latter workers [5] did find a dependence by extending their study to larger mode III/mode I ratios. Manoharan et al. [6] studied a relatively brittle steel where the mode I toughness was only slightly affected by mode III components while work by Kamat et al. [7] on an aluminum alloy based metal-matrix composite similarly showed little effect of the mode III component on mode I toughness.

Considerable work has recently been conducted to characterize the effects of reinforcement volume fraction, reinforcement size and matrix microstructure on mode I fracture toughnesses of various metal-matrix composites [8–13]. The purpose of this investigation was to characterize the fracture of an aluminum composite under combined mode I–mode III loading conditions. While the near tip deformation fields of this composite can be characterized by the stress intensity factor, no standard method is available for evaluating stress intensity factors under mixed mode loading conditions. Hence, suitably defined resolved critical stress intensity factors, denoted K_{ii} and K_{iii}, for the opening mode and transverse shear mode, respectively, were used to characterize the fracture behavior, as have been done previously [6]. The subscripts i and iii were used to emphasize that these were resolved stress intensity factors.

2. EXPERIMENTAL PROCEDURES

2.1 Material and Microstructure

The material studied was a cast and extruded aluminum alloy based, particulate reinforced metal matrix composite. The matrix was a 6061 aluminum alloy and the reinforcement consisted of 15% by volume of Al_2O_3 particulate of average size 15 μm. The composite was solution treated at 520°C for 4 hours and then artificially aged at 175°C for 2 hours to produce an underaged (UA) microstructure.

2.2 Mode I and Combined Mode I–Mode III Fracture Toughness Testing

Mode I fracture toughness tests were conducted on fatigue precracked three point bend specimens in general accordance with the applicable ASTM standard E-399 for evaluation of K_{Ic}. A schematic of the three point bend specimen is shown in Figure 1.

All combined mode fracture toughness testing was carried out using a modified three point bend specimen. The essential modification over the standard three point bend specimen is the slanted starting notch. As indicated in Figure 2, the angle θ, referred to henceforth as the crack inclination angle, is the angle between the specimen face and the crack plane. Pure mode I corresponds to a crack inclination of 90° and the geometry reduces to that of a standard three point bend specimen. As the value of θ is reduced from its pure mode I value, mode III components of the load are introduced which produce a displacement parallel to the crack front, and a range of mode I–mode III fracture behavior can be investigated. K testing was carried out for 90°, 75°, 60° and 40° to obtain a variety of mode I–mode III loading conditions.

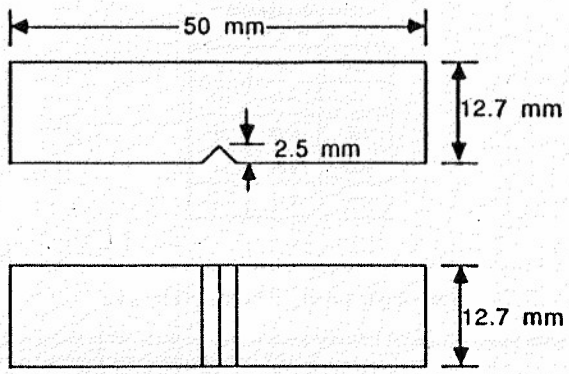

Figure 1. Schematic of mode I three point bend specimen.

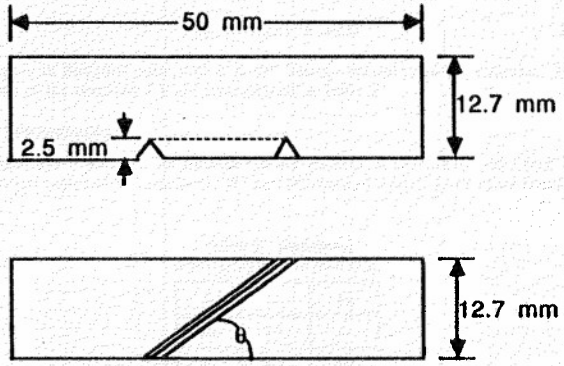

Figure 2. Schematic of combined mode three point bend specimen.

In order to ensure a reproducibly sharp precrack, ASTM standards require that specimens be fatigue precracked before fracture toughness testing. However, fatigue precracking under mixed mode conditions is difficult as the crack plane may change due to crack rotation under mixed mode conditions, which may be a particular problem for large mode III components [6]. The mixed mode three point bend specimen can be used to circumvent this problem. By aligning the crack front parallel to the loading line (achieved by rotating the specimen), the precrack can be grown in mode I and this procedure was successfully applied in this study. Fatigue precracking was monitored using DC electrical potential drop techniques.

All fracture surfaces were viewed in the SEM using secondary electrons to generate images.

3. RESULTS

3.1 Determination of the Stress Intensity Factor

The calculation of the mode I stress intensity factor was carried out in accordance with the standard procedure ASTM E-399. K_I can be calculated from the equation,

$$K_I = (PS/BW^{3/2}) \cdot f(a/w) \tag{1}$$

where

P = load
B = specimen thickness
W = specimen width
S = span
$f(a/w)$ = geometrical factor

There is no standard procedure to calculate the mixed mode stress intensity factors. However, as pointed out by Pook [3,14], apparent values of K, denoted K_A can be calculated using Equation (1) and K_I and K_{III} can then be calculated using the expressions,

$$K_I = K_A \cdot \sin^2 \theta \tag{2}$$

and

$$K_{III} = K_A \cdot \sin \theta \cdot \cos \theta \tag{3}$$

From these equations the critical mode I and mode III stress intensity factors can be evaluated.

$$K_{Ic} = (P_Q S/BW^{3/2}) \cdot f(a/w) \cdot \sin^2 \theta \tag{4}$$

Table 1. Resolved stress intensity factors ($MPa \cdot m^{1/2}$).

θ	K_{Ic}	K_{IIIc}
90	21.5	—
75	21.0	5.5
60	19.0	11.0
40	14.5	17.5

and

$$K_{IIIc} = (P_Q S/BW^{3/2}) \cdot f(a/w) \cdot \sin \theta \cdot \cos \theta \tag{5}$$

The values of the resolved critical stress intensity factors calculated using the above equations are summarized in Table 1.

If the material is assumed to be linear elastic then the stress intensity factors can be converted to their energy counterparts, the strain energy release rates which are equal to the resolved J integral values, through the equations,

$$J_{Ic} = K_{Ic}^2(1 - \nu^2)/E \tag{6}$$

$$J_{IIIc} = K_{IIIc}^2(1 + \nu)/E \tag{7}$$

where ν is Poisson's ratio and E is the Young's modulus of the material. The values of the resolved J's are summarized in Table 2.

3.2 Fractography

Figures 3–5 illustrate the fracture surface features of specimens with crack inclination angles of 90° (mode I), 75° and 60° (mixed mode). In all cases fracture

Table 2. Resolved J integral values (kJ/m^2).

θ	J_{Ic}	J_{IIIc}
90	4.1	—
75	3.9	0.4
60	3.3	1.6
40	1.9	4.1

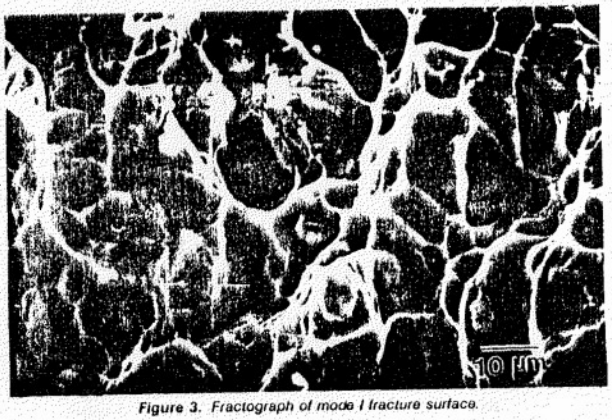

Figure 3. Fractograph of mode I fracture surface.

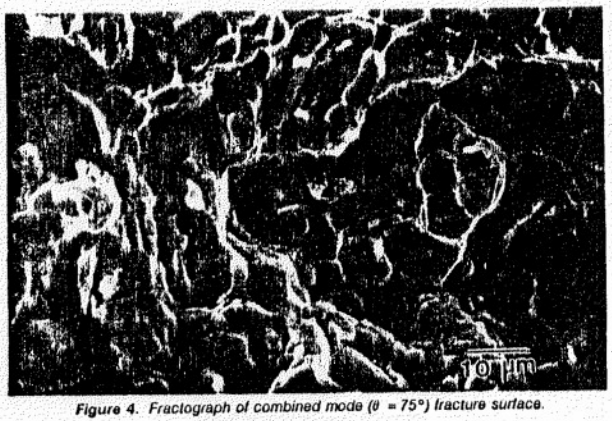

Figure 4. Fractograph of combined mode (θ = 75°) fracture surface.

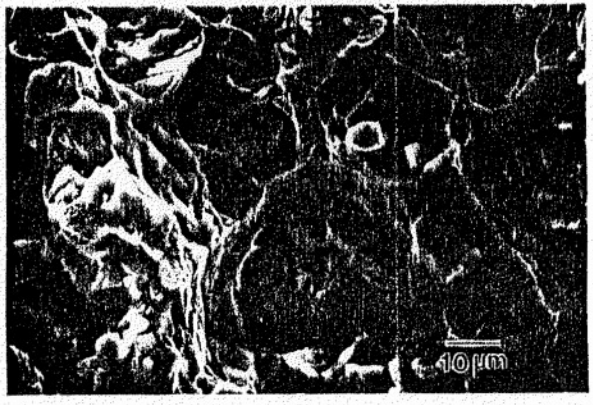

Figure 5. Fractograph of combined mode (θ = 60°) fracture surface.

occurs by cracking of the alumina particles. In other words the alumina particles underwent cleavage fracture. This can be seen from the flat nature of the alumina fracture surface and has been confirmed in other fractographic studies on this material [15]. These cracked particles serve as void intiation sites and the voids grow and coalesce by ductile failure of the matrix. The nature of the fracture surface and the dimple morphology do not exhibit any significant differences on going from the mode I loading condition to the combined mode loading conditiuns. This is probably associated with the fact that the governing fracture criterion is the stress intensity in pure mode I, the value of which does not significantly reduce as the mode II component is added. This would suggest that the normal stress and strain conditions in the vicinity of the crack tip are nearly the same for differing amounts of added mode III components, at least until $\theta = 60°$.

4. DISCUSSION

Resolved stress intensity factors are plotted as a function of the crack inclination angle in Figures 6 and 7. These figures show that K_c decreases continuously as a mode III component is added to the loading system. This decrease in the mode I contribution is, however, much less than the increase in the mode III contribution. The combined J values are plotted as a function of the crack inclination angle in Figure 8. Again, there is a relatively small drop in the mode I contribution compared tu the increase in the mode III contribution. The value of J_{mod} increases continuously from its mode I value as the mode III component is increased. Thus, at least from an energy point of view, the energy absorbed dur-

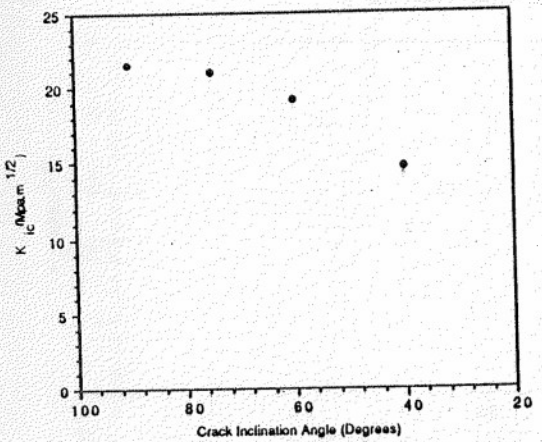

Figure 6. Resolved critical mode I K vs. crack inclination angle.

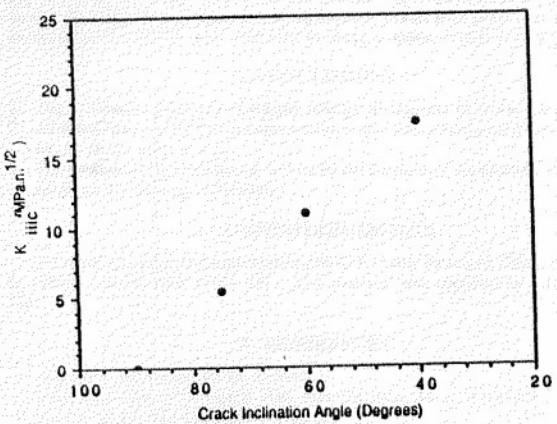

Figure 7. Resolved critical mode III K vs. crack inclination angle.

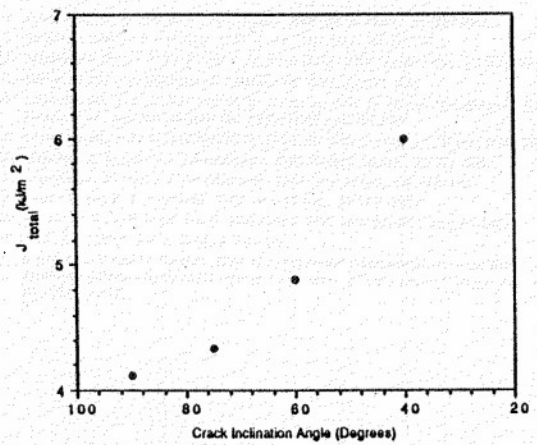

Figure 8. Total fracture energy vs. crack inclination angle.

ing mode I fracture is less than the energy absorbed during combined mode fracture. This conclusion is supported by visual observations of the crack path in the mixed-mode specimens were it was shown that the crack rotated to a mode I orientation as it propagated in an unstable fashion. In essence, the mode III component produces largely redundant plastic deformation, increasing the value of J_{total} while leaving the value J_{ss} relatively unchanged, as discussed elsewhere [6]. The relatively unchanged fracture morphology in going from mode I to mixed-mode loading conditions is also supportive of this fact.

In linear elastic materials, the fracture behavior seems to be primarily a function of the tensile stresses acting on the crack. The relative insensitivity of the K_{ss} component to mode III shear components observed in this investigation, schematically illustrated in Figure 9, supports the results of Rosenfield and Duckworth [4], Manoharan et al. [6] and Kamat et al. [7], where experiments were conducted on materials which behaved in a nearly linear elastic manner.

From the above results it would seem that under K dominance, the mode I deformation fields are not only independent of the mode III fields, they are also insensitive to them. This should be the case if the local mode I crack separation process is relatively insensitive to in-plane, mode III shear. The more brittle the material, the greater might be the insensitivity to shear stresses. In fact, Rosenfield and Duckworth [4] argue that in glass, which is closer to the brittle linear elastic continuum than most other materials, the ideal behavior involves at least a large K_{ss}/K_{ss} ratio, and possibly no influence of mode III loading at all, lead-

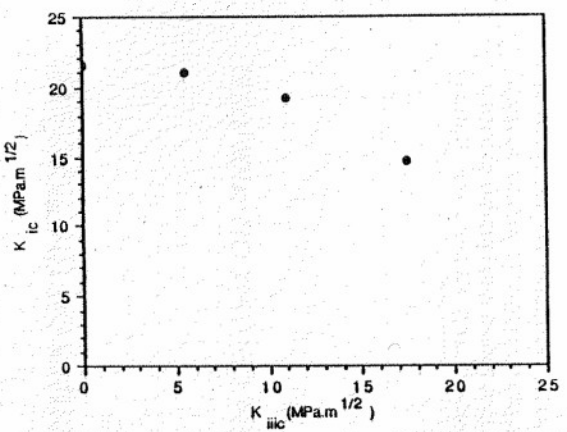

Figure 9. Resolved critical mode I K vs. resolved critical mode III K.

ing to an infinite value of K_{iiic}. In the present experiments, the composite is farther from the brittle linear elastic continuum model than glass and would be expected to be slightly more sensitive to shear stresses, which is observed.

5. CONCLUSIONS

1. The composite exhibited minimum energy dissipation in mode I fracture.
2. Addition of mode III components seems to add redundant plastic work resulting in an increase in J_{iiiic}.
3. The fracture in this composite occurs by the fracture of the alumina reinforcement for all loading conditions.

6. ACKNOWLEDGEMENTS

This work was partially supported by the U.S. Army Research Office (JJL) and by NASA NAGW 1193 (MM, JJL). The material was supplied by Alcan Int'l. Ltd.

7. REFERENCES

1. Shah, R. C. 1974. *ASTM STP 560*, 2:29–52.
2. Ueda, Y., K. Ikeda, T. Yao and M. Aoki. 1983. *Eng. Fract. Mech.*, 18:1131–1158.
3. Pook, L. P. 1971. *Eng. Fract. Mech.*, 3:205–211.

4. Rosenfield, A. R. and W. H. Duckworth. 1987. *Int. J. Fract.*, 32:R59–R62.
5. Suresh, S. and E. K. Tschegg. 1987. *J. Am. Cer. Soc.*, 70:726–733.
6. Manoharan, M., J. P. Hirth and A. R. Rosenfield. 1989. *Scripta Met.*, 23:763–766.
7. Kumar, S. V., J. P. Hirth and R. Mehrabian. 1989. 23:523–528.
8. Lewandowski, J. J., C. Liu and W. H. Hunt, Jr. 1988. In *Powder Metallurgy Composites*. M. Kumar et al., eds. Warrendale, PA: TMS-AIME, pp. 117–139.
9. Lewandowski, J. J., C. Liu and W. H. Hunt, Jr. 1989. *J. Mat. Sci. Engr.*, A107:241–255.
10. Manoharan, M. and J. J. Lewandowski. 1989. *Scripta Metall.*, 23:301–304.
11. Manoharan, M. and J. J. Lewandowski. 1990. *Acta Metall.*, 38:489–497.
12. Flom, Y. and R. J. Arsenault. 1989. *Acta Metall.*, 37:2413–2422.
13. Kumar, S. V., J. P. Hirth and R. Mehrabian. 1989. *Acta Metall.*, 37:2395–2402.
14. Pook, L. P. 1985. *Int. J. Fatigue*, 7:21–30.
15. Klimowicz, T. and K. Vecchio. 1990. In *Fundamental Relationships between Microstructure and Mechanical Properties of Metal–Matrix Composites*. P. Liaw and M. Gungor, eds. Warrendale, PA: TMS-AIME.

Materials Science and Engineering, A150 (1992) 179–186

Effect of reinforcement size and matrix microstructure on the fracture properties of an aluminum metal matrix composite

M. Manoharan and J. J. Lewandowski

Department of Materials Science and Engineering, Case Western Reserve University, Cleveland, OH 44106 (USA)

(Received July 15, 1991; in revised form September 16, 1991)

Abstract

The effects of systematic changes in reinforcement size and matrix microstructure on the crack initiation and growth toughness of a 7091 aluminum alloy reinforced with SiC particulates were studied. It is shown that changes in matrix microstructure have a significant effect on both initiation and growth toughness. The effect of reinforcement size on these properties is far less marked. These observations have been related to local microstructural parameters and the nature of the distribution of the reinforcement.

1. Introduction

Metal-matrix composites are emerging as an important class of materials in the continuing quest for improved strength, stiffness and other desirable properties. Reinforcing a ductile, tough metal with a strong ceramic is one method of achieving such an improvement in properties. Discontinuous reinforcements such as particulates or whiskers tend to produce composites with a greater degree of isotropy in properties compared with continuous fiber reinforcements. The size of the reinforcement and its volume fraction are important variables determining the properties of composites. Further, if the metallic matrix is age hardenable, suitable heat treatments can be devised to optimize properties.

Evaluation of the fracture properties of composites is essential in assessing the flaw tolerance of these materials. While there has been some work in evaluating the effects of reinforcement size and volume fraction on the fracture properties of composites based on aluminum [1] and various aluminum alloys [2–5] recent studies [2–4] have indicated significant effects of matrix microstructure on the fracture micro-mechanisms in composites based on Al-Zn-Mg-Cu matrices.

The principal objectives of the current investigation were to evaluate the effects of systematic changes in matrix microstructure and reinforcement size as well as volume fraction on the fracture initiation and growth toughness of a SiC particulate-reinforced aluminum alloy-based metal matrix composite. The age-hardenable matrix permitted the evaluation of underaged and overaged matrix microstructures of equivalent tensile properties for both the unreinforced alloy and the composite. It will be shown that the fracture initiation toughnesses in these composites are primarily controlled by changes in the matrix microstructure and yet they are relatively unaffected by reinforcement size over the range studied. These results are discussed in light of previous work [2–8] and the effects of the local fracture micromechanisms on the macroscopic fracture toughness of these materials.

2. Experimental procedures

The powder metallurgy matrix alloy composition used in this work, contains 7% Zn, 2% Cu, 2% Mg and 0.14% Zr, balance Al. Composites based on this matrix alloy and containing either 15% or 20% by volume of two sizes of reinforcement were studied. The first was F-600 grade (average size prior to blending = 13 μm) SiC particulate while the second was F-1000 grade (average size prior to blending = 5 μm) SiC particulate. The aim of designating these sizes was not to rigidly fix the particulate sizes but as a relative measure. Indeed, there is a size distribution for these reinforcements. However, as shown later in the fractographs, these relative sizes do roughly correspond to the dimple sizes. Additional details of the processing of this material via powder metallurgy techniques can be found elsewhere [2, 3]. The as-extruded materials were solution heat treated at 500 °C for 4 h, cold water quenched and artificially aged. The aging treatments were selected to

0921-5093/92/$5.00

provide equivalent matrix microhardness and 0.2% offset yield strengths in the composites for both the underaged (UA) and overaged (OA) conditions. Aging to the UA temper was conducted at 120 °C for 20 min, while the OA temper was produced by a double aging treatment: 120 °C for 24 h, followed by 170 °C for 36 h. Microstructural details produced via these heat treatments are summarized elsewhere [2, 3, 8].

Tensile tests were conducted to failure at a constant displacement rate of 0.2 mm min^{-1} (*i.e.* strain rate, 1.3×10^{-4} s^{-1}) on smooth cylindrical tensile specimens of gage length 25.4 mm and diameter 6.25 mm using an Instron model 1125 universal testing machine and strain gages affixed to the specimen surfaces. A special concentric loading fixture was utilized to minimize bending moments in the tension specimens.

Fracture properties were evaluated in general accordance with the standard procedure for J testing, ASTM E-813-81 [9]. The testing of the unreinforced material has been summarized elsewhere [2, 6]. The composite was tested using a compact tension specimen geometry, as shown in Fig. 1. A precrack of nominal root radius 30 μm was introduced using a high speed wire saw. Our earlier work [10] had shown that plane strain fracture toughness results obtained using this notch root radius were equivalent to the results using a fatigue precrack. The crack was followed optically using a travelling microscope fitted to a stage equipped with a linear variable displacement transducer (LVDT). For this purpose, the external surfaces of the specimens were polished metallographically, and the details of crack propagation were studied *in situ* with the use of a high power optical microscope connected to a video recording system. It should be noted that both aging conditions as well as reinforcement conditions were tested using specimens with identical dimensions and initial crack lengths. Since the comparisons in this study are on a relative basis, the accuracy is improved. Further, a toughness database for this material has been established using short-rod toughness specimens [2, 3], precracked three-point bend specimens [4, 7] and compact tension specimens [6]. This study extends this database for the variables of interest (*i.e.* reinforcement size and matrix aging condition) and duplicate specimens were tested for each case.

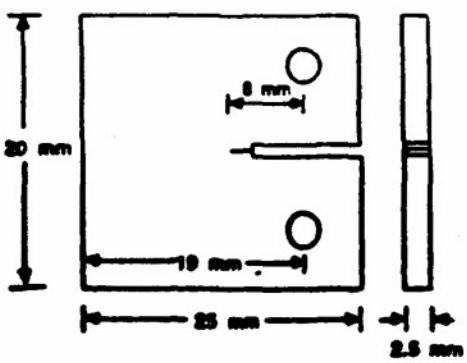

Fig. 1. Schematic of compact tension specimen.

The fracture toughness testing was carried out on an mechanical testing systems (MTS) servohydraulic-test system operated under stroke control at a cross-head speed of 25 μm min^{-1}. Displacement was measured across the crack mouth using a clip gage mounted between knife edges affixed to the front of the specimen. The load, displacement and crack length data were continuously input and stored in a PDP-11 computer.

J was calculated using the equation

$$J = \frac{A}{Bb} f(a_0/W) \tag{1}$$

where A is the area under the load-displacement record, B is the specimen thickness, b is the initial uncracked ligament, a_0 is the original crack size including fatigue precrack, and $f(a_0/W)$ is a geometry-dependent constant from ASTM-E-813-81.

The standard procedure for plane strain J integral estimation (ASTM E-813-81) was followed for the construction of the J resistance curve. This procedure involves the assumption that the blunting behavior followed the relation $J = 2\sigma_f \Delta a$, where the flow stress σ_f was set equal to $(\sigma_y + \sigma_u)/2$. The exclusion lines were then drawn at offsets of 0.15 mm and 1.5 mm respectively, parallel to the blunting line. The points that lie within these exclusion lines represent valid data points as they correspond to stable ductile crack extension. A computer program performed a linear regression analysis and fitted a straight line to these data points. The program then determined the exact point of intersection of this straight line with the blunting line and the value of J at the intersection was taken as J_{Qc}.

Once J_{Qc} is determined, it can be verified whether conditions of plane strain are satisfied. ASTM E-813-81 prescribes that plane strain conditions prevail and a valid J_{Ic} has been obtained if the following conditions are satisfied:

$$B, b > 25 J_{Ic}/\sigma_f \tag{2}$$

where B is the net thickness, b is the uncracked ligament length and σ_f is the effective flow strength. All tests conducted in this study satisfied these criteria for valid J measurement.

The crack initiation behavior of the material under these conditions is thus characterized by the values of J_{Ic}. In addition to determining J_{Ic} it was noted that, in all the tests conducted here, the J–R curve had a non-zero positive slope. The crack propagation behavior

was characterized by the tearing modulus concept of Paris *et al.* [11]. The dimensionless value of tearing modulus is given by the expression

$$T = \frac{E}{\sigma_f^2}\frac{dJ}{da} \quad (3)$$

where dJ/da is the slope of the J resistance curve between Δ_c and Δ_{exc}, E is Young's modulus of the material, and σ_f is the flow stress of the material in tension ($\sigma_f = (\sigma_y + \sigma_u)/2$).

As mentioned earlier, crack propagation in the composite was monitored *in situ*. In addition, some of the tests were stopped at periodic increments of crack growth, were unloaded and the specimens transferred to a JEOL 35-CF scanning electron microscope. The unloading compliance was recorded as an additional measure of crack length while the crack path on the external surfaces were examined at high magnification. The fracture surfaces were also examined for all specimens using the scanning electron microscope.

3. Results

Table 1 summarizes tensile test data for the unreinforced and 20 vol.% reinforced material for the as-solution-treated, UA and OA materials. Figure 2 shows true stress–true plastic strain curves in the low strain regime for the 20 vol.% composite for both aging conditions. It can be seen that the yield strength is nearly identical for both the aging conditions and reinforcement sizes. However, the composite reinforced with 5 μm SiC seems to have a somewhat higher work hardening rate as discussed elsewhere [12].

Table 2 summarizes J_{Ic} and tearing modulus values for both the unreinforced material and the composite for both matrix aging conditions (*i.e.* UA and OA) while Figs. 3 and 4 show the J–R curves obtained for UA and OA composite materials reinforced with both

TABLE 1. Tensile properties of unreinforced and composite materials

Material	Yield stress (MPa)	Ultimate tensile strength (MPa)	Elongation (%)	Reduction in area (%)
ST, unreinforced	150	300	16	—
ST, 13 μm, 20% SiC	210	375	12	—
UA, unreinforced	509	638	20	21
UA, 5 μm, 20% SiC	379	496	5	8
UA, 13 μm, 20% SiC	381	502	4	8
OA, unreinforced	553	594	19	38
OA, 5 μm, 20% SiC	418	473	3	7
OA, 13 μm, 20% SiC	406	459	3	7

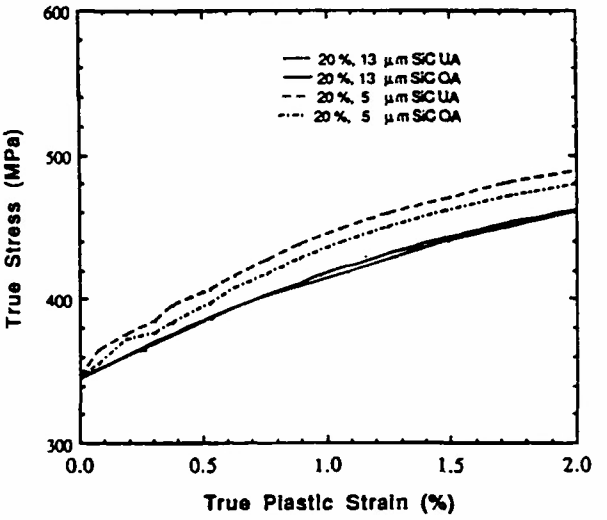

Fig. 2. True stress–true plastic strain curves: ···, 20% 13 μm SiC UA; ——, 20% 13 μm SiC OA; – – –, 20% 5 μm SiC UA; —·—, 20% 5 μm SiC OA.

TABLE 2. Fracture properties of unreinforced and composite materials

Material	J_{Ic} (kJ m^{-2})	δ (μm)	λ (μm)	Tearing modulus
UA, unreinforced	31	—	—	6.0
UA, 5 μm, 15% SiC	15	40	10	1.0
UA, 13 μm, 15% SiC	16	39	26	2.0
UA, 5 μm, 20% SiC	11	29	9	1
UA, 13 μm, 20% SiC	11	30	23	2.0
OA, unreinforced	31.5	—	—	7.0
OA, 5 μm, 15% SiC	5.5	12	10	0.1
OA, 13 μm, 15% SiC	7.4	15	26	1.0
OA, 5 μm, 20% SiC	4.1	9	9	0.1
OA, 13 μm, 20% SiC	5.5	13	23	1.0

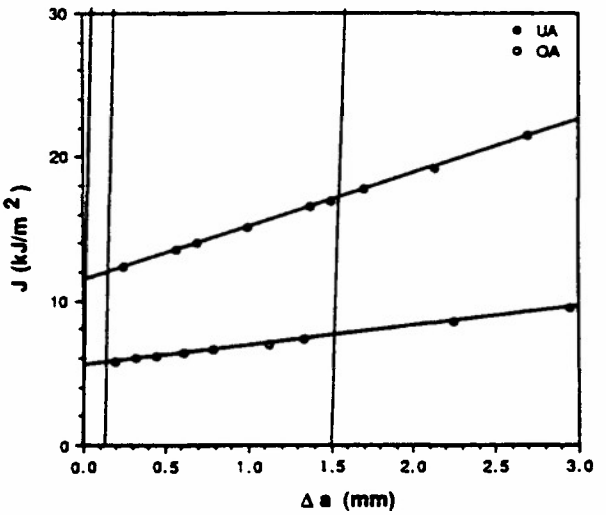

Fig. 3. Plot of the J–Δa curve for the composite reinforced with 20 vol.% 13 μm SiC: ●, UA; ○, OA. The blunting line and exclusion lines are shown.

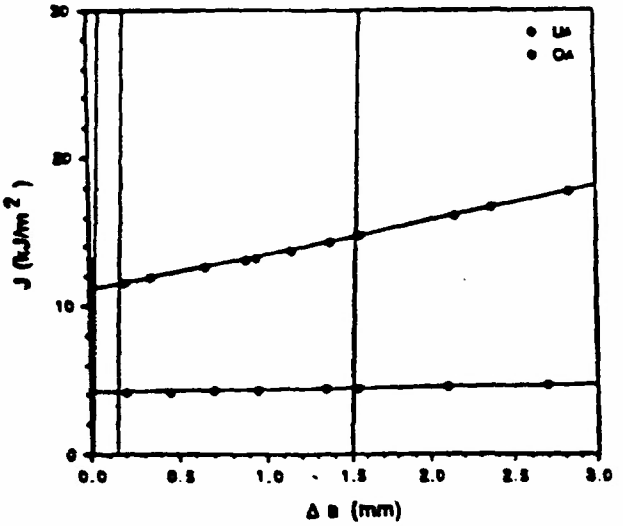

Fig. 4. Plot of the J–Δa curve for the composite reinforced with 20 vol.% 5 μm SiC: ●, UA; ○, OA. The blunting line and exclusion lines are shown.

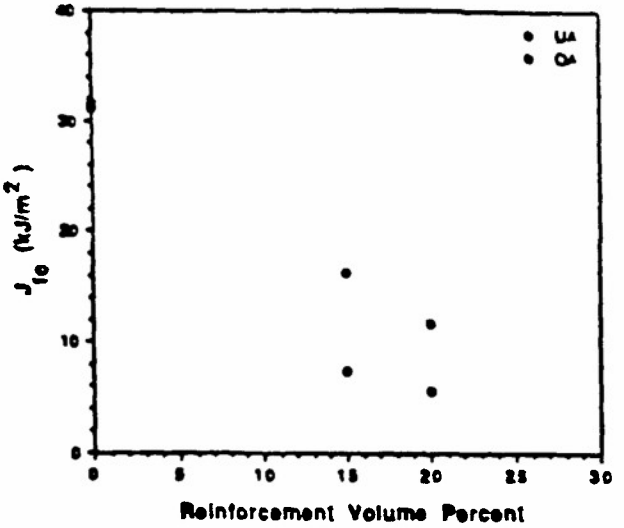

Fig. 5. Plot of J_{Ic} vs. reinforcement per cent for the composite reinforced with 13 μm SiC: ●, UA; ○, OA.

5 and 13 μm SiC. It is shown that the J_{Ic} values were nearly identical for the unreinforced materials, and that the tearing modulus of the OA unreinforced material is slightly higher than that of the UA material. In general, for a given condition, the average spread in the values is less than 5%.

Figures 5 and 6 show the effects of aging condition and reinforcement volume fraction on the initiation toughnesses for the 5 μm and 13 μm SiC reinforcements respectively. It can be seen for the materials reinforced with both the 5 and 13 μm SiC that, while the UA material exhibits a nearly linear decrease in J_{Ic} as the volume fraction of SiC increases from zero to 20%, the OA material shows a much more rapid and non-linear decrease over the same range of volume fractions. Further, the J_{Ic} values for the OA composite are about 50% lower than those for the UA composite at the given volume fractions. It can clearly be seen that the effect of aging condition is much greater than the effect of reinforcement size in determining the fracture toughnesses of these composites in the range of particle sizes and volume fractions studied.

The tearing modulus of the OA composite is also significantly lower than that of the UA composite, although these values appear to be independent of volume fraction in the range 15–20 vol.% reinforcement, for a given reinforcement size. The composite reinforced with 5 μm SiC exhibited lower fracture growth toughness than the composite reinforced with 13 μm SiC for a given aging condition.

Although the fractographic details were not significantly different for the unreinforced materials, fracture mechanisms operative in the composite exhibited a

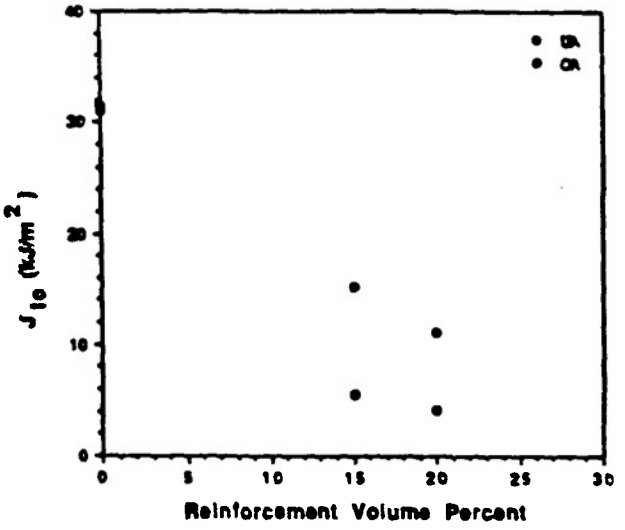

Fig. 6. Plot of J_{Ic} vs. reinforcement volume per cent for the composite reinforced with 5 μm SiC: ●, UA; ○, OA.

strong dependence on the matrix aging condition. In general, the fracture surface essentially consisted of a bimodal distribution of dimples with the larger dimples associated with the SiC particles and the smaller dimples associated with the ductile fracture of the alloy. Figure 7 illustrates fracture surfaces of the 13 and 5 μm UA composites. In the UA composite reinforced with 13 μm SiC, matching surface fractography showed that the fracture surfaces exhibited fractured SiC particles as shown elsewhere [2, 3]. In the OA composite reinforced with 13 μm SiC a similar analysis found less fractured SiC particles, with failure pre-

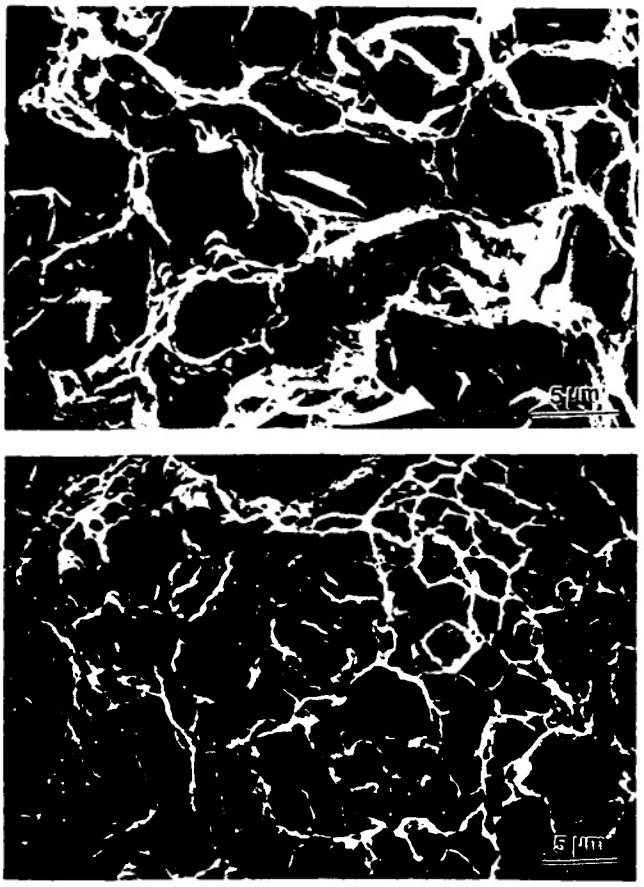

Fig. 7. SEM fractographs showing fracture surfaces of the UA 13 μm and UA 5 μm materials.

dominantly in the matrix and near the SiC–matrix interfaces. The details of these fractographic observations are summarized elsewhere [2–4]. In the case of the composite reinforced with 5 μm SiC such a statistical analysis is complicated by the smaller size of the particles and the associated dimples. However, qualitative observations coupled with the trends in the fracture toughness results seem to indicate similar differences in micromechanisms between UA and OA composites. A more complete analysis of the effects of particulate size and matrix microstructure on damage evolution in these materials is summarized elsewhere [13].

4. Discussion

4.1. Tensile properties

A number of approaches have been taken in the literature to model the strength of metal matrix composites. One of the approaches is the modified shear lag theory [14] which derives its basis from fiber-reinforced composites. It essentially involves the concept of a load transfer from the matrix to the fiber via the fiber interface [15]. However, as pointed out by Humphreys [15], as the fibers become shorter, modifications have to be made for the factors governing the load transfer from matrix to fiber.

Humphreys [15] has indicated that the addition of a brittle reinforcement in high strength aluminum alloys may even decrease the yield stress. Indeed in the present composite, this was found to be the case. One plausible explanation is that, as composites with these high strength matrices are strained, the stresses on the reinforcement become large. Fracture can then occur in the reinforcement in the presence of a pre-existing flaw in the reinforcement, probably formed during earlier processing. Once the reinforcement fractures, the net load-carrying capacity of the composite decreases and thus yield stress might decrease. Recent experimental work on sequentially strained specimens has indicated that the nucleation of reinforcement cracking is very matrix and particle size dependent [13]. Levy and Papazian [16] have provided finite element analyses that additionally indicate that initial flow is promoted during loading near stress concentrations caused by the presence of the reinforcements, while it is also possible that the mismatch between reinforcement and matrix leads to a large stress concentration near the reinforcement and the matrix in that region fails prematurely. In lower strength matrices, the stresses reached locally might not be large enough for either of these effects to occur, leading to strength improvement through the processes outlined earlier. In order to evaluate the possibility of such effects, both the unreinforced and composite materials were heat treated to the as-solution-treated condition. In this condition, the matrix strength is low due to the absence of hardening precipitates. The addition of the SiC in this case leads to an improvement in both the yield and ultimate tensile strength of the material. This suggests that the lower values obtained for the UA and OA composites, which have higher strength matrices, is at least in part due to the reasons outlined earlier.

The higher work hardening rate in the composites with the 5 μm SiC reinforcement compared with the 13 μm reinforcement can be qualitatively understood by a model similar to that proposed by Kamat *et al.* [5], although the magnitudes of such work hardening rates are currently under investigation [12]. They suggest that, at low strains, dislocations tangles form around the particles due to plastic incompatibility. The tangles eventually link up to form a dislocation cell structure with a cell size related to interparticle spacing. Such a model would then lead to a flow stress inversely proportional to interparticle spacing, which would qualitatively explain the higher work hardening rate in the 5 μm composite, as shown elsewhere [12].

4.2 Fracture toughness

The primary aim of this investigation was to study the effects of matrix aging condition and reinforcement size on the fracture behavior of these composites. The fracture toughness of precipitation- or dispersion-strengthened aluminum alloys has been well investigated [17]. While it has often been observed that the fracture toughness of monolithic aluminum alloys in the OA condition is somewhat lower than that obtained in the UA condition, this is not always observed [18]. Recent work [2, 3, 6] on monolithic powder-metallurgy-processed materials has shown nearly identical toughness in UA and OA conditions of equivalent strength.

The fracture toughness of pure aluminum-based particulate-reinforced metal matrix composites has been studied by Flom and Arsenault [1] while the behavior of Al–Mg–Cu-based composites in the annealed condition has been investigated by Kamat *et al.* [5]. Flom and Arsenault concluded that submicron oxide particles, inclusions *etc.* are responsible for the microvoid coalescence mechanisms of fracture in the SiC–Al composites studied [1] and found that an increase of SiC particle size from 2.4 to 20 μm did not improve the fracture initiation toughness. Kamat *et al.* [5] concluded that fracture in an Al_2O_3-particulate-reinforced Al–Mg–Cu alloy is controlled by the development of a dislocation cell structure of a size comparable with the interparticle spacing and that fracture occurs by Al_2O_3 fracture. The fracture toughness, for a reinforcement volume fraction of 2–20%, was found to increase with particle spacing provided that the particle size was less than a critical value, which was approximately 15 μm. They concluded that this critical value correlates with a particle which when cracked presents a microcrack that exceeds the matrix toughness locally. Their stress intensity values, at least for small sizes of Al_2O_3 and lower volume fractions, were compatible with a Rice and Johnson [19] type of model.

In the present investigation, it was found that the critical J integral value is a strong function of matrix aging condition but relatively independent of SiC particle size for the limited sizes tested. Table 2 summarizes the observed J_{Ic} values. Initial attempts at rationalizing these results have focussed on a model first suggested by Rice and Johnson [19] and used by Kamat *et al.* [5]. In such a model all particles are considered to crack or decohere ahead of the major crack tip and at a low strain value. Experimental observations of the crack tip regions in these materials have been provided elsewhere [3, 6, 20]. The region of plastic flow is limited to a volume of width δ, a value which could presumably correspond to interparticle spacing. If such a relation were to hold, the following equation applies:

$$\frac{J_{Ic}}{\sigma_1} = \delta \tag{4}$$

For such a homogeneous arrangement of particles, the interparticle spacing λ can be estimated from the microstructure through the relation [21]

$$\lambda = 0.77\, d V^{-1/2} \tag{5}$$

where d is the average particle size and V is the volume fraction of the reinforcement. Table 2 summarizes the values of λ and δ for all the aging conditions and particle sizes studied while typical fracture surfaces for the UA materials reinforced with 13 and 5 μm SiC were shown previously in Fig. 7 and indicate a decrease in dimple size with decreasing particle size.

It can be seen from Table 2 that the value of δ predicted by the model corresponds reasonably to the interparticle spacing λ for the UA composite reinforced with 13 μm SiC. This would suggest that the region of intense plastic strain is confined to a region corresponding to the interparticle spacing and that fracture proceeds by a sequential link up of fractured SiC particles in this material. However, in the UA composite reinforced with 5 μm SiC, the value of δ is unchanged compared with the 13 μm composite but the interparticle spacing is much smaller. One potential reason for this difference could be due to differences in the amount of clustering of SiC particles between the two cases (*i.e.* 5 μm *vs.* 13 μm). One measure of the degree of clustering is provided by comparing the distribution of local area fractions of reinforcements observed with that expected for a random distribution. Such an analysis can be performed by using the Dirichlet tesselation technique as described elsewhere [22]. Analyses conducted on these materials [2, 3] have indicated that in a comparative sense the 5 μm composite is more clustered than the 13 μm composite. In a qualitative sense, these regions of clustered particles can act as centers of strain localization and the critical fracture distance and the region of intense plastic strain can then be thought of as being related to intercluster spacing as opposed to interparticle spacing. The magnitude of the effect of clustering also seems to depend on the mechanisms of the local fracture events as the clustering seems to have a larger effect on the fracture of the 5 μm UA composite while the effect on the 5 μm OA composite seems to be smaller, since the values of δ and λ seem to agree more closely in this case. This is presumably related to the weakening of the near-interface regions in the OA composite which might compensate for the stress enhancement produced by clustering. Thus fracture in this composite is controlled by a number of interrelated factors in the matrix microstructure and reinforcement distribution. Work is progressing in an attempt to describe the effects

of clustering on various phenomena [23], including fracture.

While the lack of dependence of the fracture initiation toughness on particle size may be related to the differing amounts of clustering present in the two materials, the differences in the fracture toughness between UA and OA composites is related to the differences in local failure mechanisms operating in these two cases. As reported earlier, in the UA composite, fracture occurs predominantly by the fracture of SiC particulates, while the OA composite showed failure predominantly in the matrix and near the SiC–matrix interfaces. The difference in the fracture energy as measured by the J integral values can then be correlated with the different energy requirements for these local fracture events. Presumably, weakening of the near-interface region in the OA composite in combination with easier void nucleation in the matrix leads to the lower total fracture energy reflected in both the fracture initiation and growth toughnesses obtained for the OA material. Thus the local fracture micromechanisms appear to play an important role in determining macroscopic fracture properties. In this composite, fracture property predictions based solely on the basis of uniaxial properties might be an oversimplification. An attempt at measuring the effects of microstructural changes on the interfacial strength has been made using static friction experiments with single-crystal SiC and the present aluminum alloy. In that work it was shown that similar heat treatments produced a sequential decrease in the strength of the interfaces on going from the UA to OA condition [24].

It should also be pointed out that the values of the J integral scale inversely with increases in volume fraction from 15 to 20% for both reinforcement sizes and all aging conditions. It is thus possible that the fracture properties of these composites can be estimated using an energy-based approach as a sum of the energy to fracture the matrix and the energy required to fracture the SiC or decohere the SiC–matrix interface. However, the OA material does exhibit a lower absolute value of initiation toughness for both reinforcement sizes. This would also indicate that the reinforcement–matrix interfaces and the aging precipitates in the matrix and at grain boundaries in the OA materials provide lower energy sources for void initiation than they do in the UA material where SiC particle cracking predominate.

The tearing modulus values seem to be relatively independent of the reinforcement volume fraction but strongly dependent on matrix aging condition. The tearing modulus of the material reinforced with 13 μm SiC is higher than the material reinforced with 5 μm SiC. The relative independence of volume fraction might be due to the small changes in volume fraction studied. As noted by Ritchie and Thompson [25] and as shown by Vasudevan *et al.* on Al–Li alloys [26] and by the present authors in similar composites [6], changes in microstructure can produce markedly different changes in crack initiation and growth characteristics. The decrease in tearing modulus, measured as a difference, is nearly the same for both UA and OA conditions as reinforcement size is increased. The tearing moduli are strongly dependent on matrix aging condition. As with the initiation toughnesses, the tearing modulus of the OA composite is less than 50% of the UA composite. Once again, this observation indicates that the relative energies of local fracture mechanisms must be taken into account in any analysis of the macroscopic crack growth toughness. Recent work [7, 27] on other aluminum alloy composites have additionally indicated that the toughness response to microstructural changes may be different for other matrices, while decreases in toughness may also occur without a change in the fracture behavior of the reinforcement [27].

5. Conclusions

(1) While UA and OA composites exhibited similar tensile properties at identical volume fractions, the fracture initiation toughness (as measured by J_{Ic}) of the UA composite was about twice that of the OA composite for composites reinforced with both 5 μm SiC and 13 μm SiC.

(2) The UA composite exhibited a nearly linear decrease in J_{Ic} as the volume fraction of SiC was increased from zero to 20% while the OA composite exhibited a more rapid initial decrease in J_{Ic} over the same range of volume fractions for both 5 and 13 μm SiC reinforcements.

(3) The value of J_{Ic} showed only a minor dependence on the size of the reinforcement in the range studied.

(4) The crack growth toughness (as measured by the tearing modulus) of the UA composite was greater than that of the OA composite for both the reinforcement sizes.

(5) The tearing modulus of the composite reinforced with 13 μm SiC was higher than that of the composite reinforced with 5 μm SiC for both UA and OA conditions.

(6) Associated with this decrease in the crack initiation and growth toughnesses in going from a UA to a OA microstructure was a transition in the local fracture mode from SiC fracture (UA) to failure near the SiC–matrix interface (OA). This was shown statistically for the composite reinforced with 13 μm SiC and

qualitatively for the composite reinforced with 5 μm SiC

Acknowledgments

The authors would like to thank W. Hunt, Jr., of ALCOA for supply of the material. This work was supported by the U.S. Army Research Office (DAAL03-89-K-0068) (M. Manoharan, J. J. Lewandowski) with partial support from the National Science Foundation (NSF-DMR-89-58326) (J. J. Lewandowski). The authors are also thankful to Professor J. P. Hirth for his comments and suggestions.

References

1 Y. Flom and R. J. Arsenault, *Acta Metall.*, *37* (1989) 2413.
2 J. J. Lewandowski, C. Liu and W. H. Hunt, Jr., in P. Kumar, K. Vedula and A. Ritter (eds.), *Processing and Properties of Powder Metallurgy Composites*, Metallurgical Society of AIME, Warrendale, PA, 1988, p. 117.
3 J. J. Lewandowski, C. Liu and W. H. Hunt, Jr., *Mater Sci. Eng A*, *107* (1989) 241.
4 M. Manoharan, C. Liu and J. J. Lewandowski, in K. Salama, K. Ravi-Chander, D. M. R. Taplin and P. Rama Rao (eds.), *Proc. Int. Conf. on Fracture*, Pergamon, Oxford, 1989, p. 2977.
5 S. V. Kamat, J. P. Hirth and R. Mehrabian, *Acta Metall.*, *37* (1989) 2395.
6 M. Manoharan and J. J. Lewandowski, *Acta Metall.*, *38* (1990) 489.
7 M. Manoharan and J. J. Lewandowski, *Scripta Metall.*, *23* (1989) 301.
8 M. Strangewood, C. A. Hippsley and J. J. Lewandowski, *Scripta Metall.*, *24* (1990) 1483.
9 *ASTM Annual Book of Standards*, American Society for Testing and Materials, Philadelphia, PA, 1987, p. 713.
10 M. Manoharan and J. J. Lewandowski, *Int. J. Fract.*, *40* (1989) R34.
11 P. C. Paris, H. Tada, A. Zahoor and H. Ernst, *Am. Soc. Test. Mater., Spec. Tech. Publ.*, *668* (1979) 5.
12 J. J. Lewandowski, D. S. Liu and C. Liu, *Scripta Metall.*, *25* (1991) 21.
13 P. M. Singh and J. J. Lewandowski, *Metall. Trans. A*, submitted for publication.
14 V. C. Nardone and K. M. Prewo, *Scripta Metall.*, *20* (1986) 43.
15 F. J. Humphreys, in S. I. Anderson *et al.* (eds.), *Mechanical and Physical Behavior of Metallic and Ceramic Composites*, Riso National Laboratory, Charlottesville, VA, 1988, p. 51.
16 A. Levy and J. Papazian, *Metall. Trans. A*, *21* (1990) 411.
17 G. G. Garrett and J. F. Knott, *Metall. Trans. A*, *9* (1978) 1187.
18 J. T. Staley, *Proc. 10th Symp. on Naval Structural Mechanics — Fracture Mechanics*, University of Virginia, Roskilde, Denmark, 1978, p. 671.
19 J. R. Rice and M. A. Johnson, in M. F. Kanninen, H. Lilholt and O. B. Pedersen (eds.), *Inelastic Behavior of Solids*, McGraw-Hill, New York, NY, 1969, p. 641.
20 M. Manoharan and J. J. Lewandowski, *Scripta Metall.*, *23* (1989) 1801.
21 G. LeRoy, J. D. Embury, G. Edwards and M. F. Ashby, *Acta Metall.*, *29* (1981) 1509.
22 P. J. Wray, O. Richmond and H. G. Morrison, *Metallography*, *16* (1983) 39.
23 J. D. Embury, *Metall. Trans A*, *16* (1985) 2191.
24 R. Haaland, G. Chortiner and G. Michal, in P. Liaw and M. Gungor (eds.), *Fundamental Relationships Between Microstructure and Mechanical Properties of Metal-matrix Composites*, Metallurgical Society of AIME, Warrendale, PA, 1990, p. 779.
25 R. O. Ritchie and A. W. Thompson, *Metall. Trans. A*, *16* (1985) 233.
26 A. K. Vasudevan, E. A. Ludwiczak, S. F. Bauman, P. R. Howell, R. D. Doherty and M. M. Kerskar, *Mater. Sci. Technol.*, *2* (1986) 1205.
27 T. Klimowicz and K. Vecchio, in P. Liaw and M. Gungor (eds.), *Fundamental Relationships Between Microstructure and Mechanical Properties of Metal-matrix Composites*, Metallurgical Society of AIME, Warrendale, PA, 1990, p. 255.